Physiological C-terminal truncation of α-synuclein potentiates the prion-like formation of pathological inclusions

Received for publication, August 28, 2018, and in revised form, October 11, 2018 Published, Papers in Press, October 16, 2018, DOI 10.1074/jbc.RA118.005603

Zachary A. Sorrentino[‡§], Niran Vijayaraghavan[‡§], Kimberly-Marie Gorion[‡§], Cara J. Riffe[‡§], Kevin H. Strang[‡§], Jason Caldwell[‡§], and Benoit I. Giasson[‡§¶1]

From the [‡]Department of Neuroscience, the [§]Center for Translational Research in Neurodegenerative Disease, and the [¶]McKnight Brain Institute, College of Medicine, University of Florida, Gainesville, Florida 32610

Edited by Paul E. Fraser

α-Synuclein (αsyn) aggregates into toxic fibrils in multiple neurodegenerative diseases where these fibrils form characteristic pathological inclusions such as Lewy bodies (LBs). The mechanisms initiating αsyn aggregation into fibrils are unclear, but ubiquitous post-translational modifications of αsyn present in LBs may play a role. Specific C-terminally (C)-truncated forms of αsyn are present within human pathological inclusions and form under physiological conditions likely in lysosome-associated pathways, but the roles for these C-truncated forms of αsyn in inclusion formation and disease are not well understood. Herein, we characterized the *in vitro* aggregation properties, amyloid fibril structures, and ability to induce full-length (FL) αsyn aggregation through prion-like mechanisms for eight of the most common physiological C-truncated forms of αsyn (1–115, 1–119, 1–122, 1–124, 1–125, 1–129, 1–133, and 1–135). *In vitro*, C-truncated αsyn aggregated more readily than FL αsyn and formed fibrils with unique morphologies. The presence of C-truncated αsyn potentiated aggregation of FL αsyn *in vitro* through co-polymerization. Specific C-truncated forms of αsyn in cells also exacerbated seeded aggregation of αsyn. Furthermore, in primary neuronal cultures, co-polymers of C-truncated and FL αsyn were potent prion-like seeds, but polymers composed solely of the C-truncated protein were not. These experiments indicated that specific physiological C-truncated forms of αsyn have distinct aggregation properties, including the ability to modulate the prion-like aggregation and seeding activity of FL αsyn. Proteolytic formation of these C-truncated species may have an important role in both the initiation of αsyn pathological inclusions and further progression of disease with strain-like properties.

Lewy body dementia (LBD)[2] and Parkinson's disease (PD) are pathologically characterized by neuronal Lewy body (LB) inclusions composed of amyloidogenic α-synuclein (αsyn), along with associated gliosis and neurodegeneration (1–4). The propensity of αsyn to aggregate into β-sheet–rich fibrils has been posited to play a crucial role in the initiation and progression of disease, as a number of familial αsyn missense mutants that cause hereditary PD/LBD accelerate this aggregation process (5–9). Furthermore, these aggregation-prone αsyn mutants have been successfully utilized to generate robust murine models of disease (10, 11). The resulting αsyn fibrils found in LB inclusions have the capacity to recruit endogenous αsyn into further fibrils through a prion-like process termed conformational templating (2, 12); this property of fibrillar αsyn in combination with its observed toxicity and ability to spread intercellularly suggests that αsyn fibrils may underlie disease pathogenesis (13–16).

The importance of αsyn fibrils to disease progression has been established; however, mechanisms by which initial fibrils form are not well-understood. In the absence of pre-existing fibrils to catalyze αsyn aggregation, initial fibrils are posited to slowly assemble from monomeric αsyn (17–19). This aggregation process can be promoted by toxic cellular insults, notably those that impair lysosomal chaperone-mediated autophagy, which is the major clearance pathway for physiologic and fibrillar αsyn (20–23). Specifically, impaired lysosomal function as is seen in risk factors for PD, including glucocerebrosidase insufficiency, lysosomal storage diseases, or aging in general, may promote such toxic aggregation (24–29). In particular, lysosomal impairment may promote formation of C-terminally truncated αsyn through incomplete lysosomal proteolytic digestion, which has been demonstrated *in vitro* and in cell culture (22, 30–34). C-terminal truncation of αsyn has been repeatedly shown to promote *in vitro* fibril formation more promptly than even αsyn harboring the familial A53T mutation or any other post-translational modification (35–41). Indeed, monomers of C-truncated αsyn will self-assemble into fibrils resembling those found in LBs with minimal incubation; comparatively, full-length (FL) αsyn requires days of continual incubation along with vigorous shaking to form characteristic

This work was supported by National Institutes of Health Grants R01NS089022 and R21NS102685. The authors declare that they have no conflicts of interest with the contents of this article. The content is solely the responsibility of the authors and does not necessarily represent the official views of the National Institutes of Health.

This article contains Figs. S1–S4.

[1] To whom correspondence should be addressed: BMS J483/CTRND, 1275 Center Dr., Gainesville, FL 32610. Tel.: 352-273-9363; E-mail: bgiasson@ufl.edu.

[2] The abbreviations used are: LBD, Lewy body dementia; LB, Lewy body; PD, Parkinson's disease; αsyn, α-synuclein; FBS, fetal bovine serum; FL, full-length; pSer[129], phosphorylated Ser[129] α-synuclein; TBS, Tris-buffered saline; ThT, thioflavin T; N- and C-truncated, N- and C-terminally truncated, respectively; C-truncation, C-terminal truncation; DAPI, 4′,6-diamidino-2-phenylindole; E, embryonic day; ANOVA, analysis of variance.

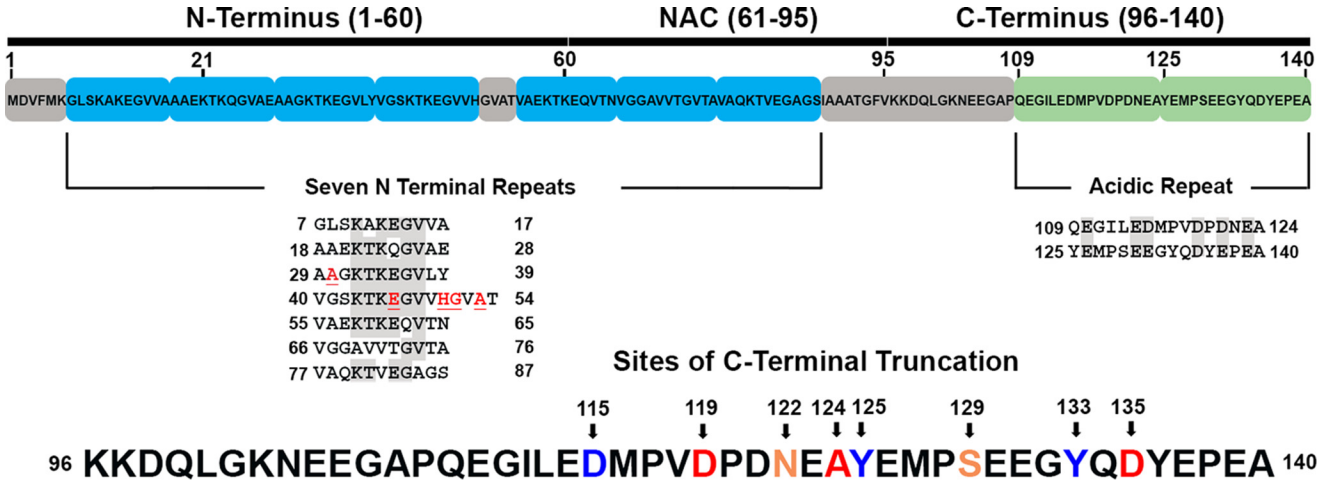

Figure 1. Depiction of the structural domains of αsyn and the sites of physiologic C-terminal truncation used in this study. Shown is a layout of the three principle regions of the FL 1–140 isoform of human αsyn. The amphipathic N terminus harbors a number of imperfect repeats important in generating helical structure for membrane interactions; the locations of all familial disease–causing mutations are in this region and shown in *red*. The hydrophobic NAC region is crucial in generating the core of fibrils and is thought to mediate prion-like conformational templating. The acidic C terminus contains two negatively charged repeats; its 15 negatively charged residues, 5 prolines, and long-range interactions with the NAC to shield it from pathologic aggregation all act as inhibitors of fibril formation. C-terminal truncations found to occur in human cells, isolated from LBs, and used in this study are indicated by *arrows* and *numbered* at the cleaved residue.

fibrils (36, 37). Unlike rare familial disease–causing mutant forms of αsyn, C-truncated species are presumably found in all neurons, as ubiquitous lysosomal proteases are implicated in their formation (22, 30–34).

Immunodetection of pathologic αsyn from patient samples reveals the striking role C-truncated αsyn may have in the pathophysiology of PD and LBD. Brain lysate from PD and LBD patients demonstrates an abundance of C-truncated αsyn in the detergent-insoluble, aggregated fractions compared with controls; truncated αsyn is estimated to represent 10–25% of total αsyn within these LB extracts (42–46). Furthermore, truncation-specific antibodies have been used to localize C-truncated αsyn to the center of LBs where FL αsyn occupies a more circumferential location, suggesting an initiating role for C-truncated αsyn in the generative processes of these inclusions (47, 48).

Truncated forms of αsyn are elevated in PD and LBD, but only limited studies have gone beyond this association and explored mechanistic implications for disease. Overexpression of some C-truncated forms of αsyn in cell culture, in *Drosophila*, and in murine models mainly under the rat TH promoter has demonstrated that these truncations tend to be more toxic than the FL protein, and the mouse models have displayed motor symptoms, filamentous neuronal inclusion formations, and dopaminergic dysfunction (34, 43, 49–57). The mitochondrial toxicity of these truncated species may also be critically important in mediating cellular demise (58). As useful as these studies have been, many of these models have used truncations not commonly found in human disease or have examined the truncations in the absence of FL human αsyn. Herein, a full panel of the C-terminally truncated αsyn proteins confirmed to exist in LBs and form in human cells (32, 45, 46) are examined in cultured cells for their propensity to aggregate and do so synergistically with FL αsyn. Additionally, the ability of preformed C-truncated αsyn fibrils to further αsyn aggregation in neuronal-glial culture is also studied.

Results

Physiologic C-truncation of αsyn readily promotes aggregation in vitro

To investigate differences in aggregate formation kinetics *in vitro* between human FL αsyn and the eight major C-truncated αsyn species that form under physiologic conditions (Fig. 1), monomers of each were diluted to 150 μM in PBS and incubated at 37 °C with shaking over the course of 96 h. The rate of αsyn amyloid formation was monitored using fluorometry, as αsyn fibrils are amyloidogenic (59), and their formation can be quantified using the fluorescent amyloid binding dyes K114 and thioflavin T (ThT) (59, 60). K114 is derived from the structure of Congo Red and binds a different amyloid site than ThT (60). Fluorometry readings were normalized to the fraction of insoluble protein at the final 96-h time point (Fig. S1, *A* and *B*). Serial fluorometric readings with both ThT and K114 (Fig. 2, *B* and *C*) revealed a sigmoidal transition from soluble monomers to insoluble fibrils for all C-truncated forms of αsyn, which is characteristic of *in vitro* amyloid formation processes (17). The 1–115, 1–119, and 1–125 αsyn truncations showed substantially increased aggregation rates compared with FL αsyn using ThT, which is evidenced by their left-shifted sigmoidal curves. At just 6 h of incubation, these three truncations had attained ~50% or more of their eventual peak ThT fluorescence, whereas comparatively, the FL αsyn did not reach this level until at least 48 h. The 1–122, 1–124, and 1–129 αsyn truncations fibrillized more readily than FL αsyn, as evidenced by significantly increased normalized ThT fluorescence at 24 h (Table 1); however, the effect was less compared with the 1–115, 1–119, and 1–125 αsyn truncations. Last, the 1–133 αsyn and 1–135 αsyn demonstrated no significant difference in aggregation measured by fluorometry compared with FL αsyn at any time point (Table 1). In addition to the rate of formation, the total extent of aggregation for each C-truncated form of αsyn was assessed using centrifugal sedimentation analysis at

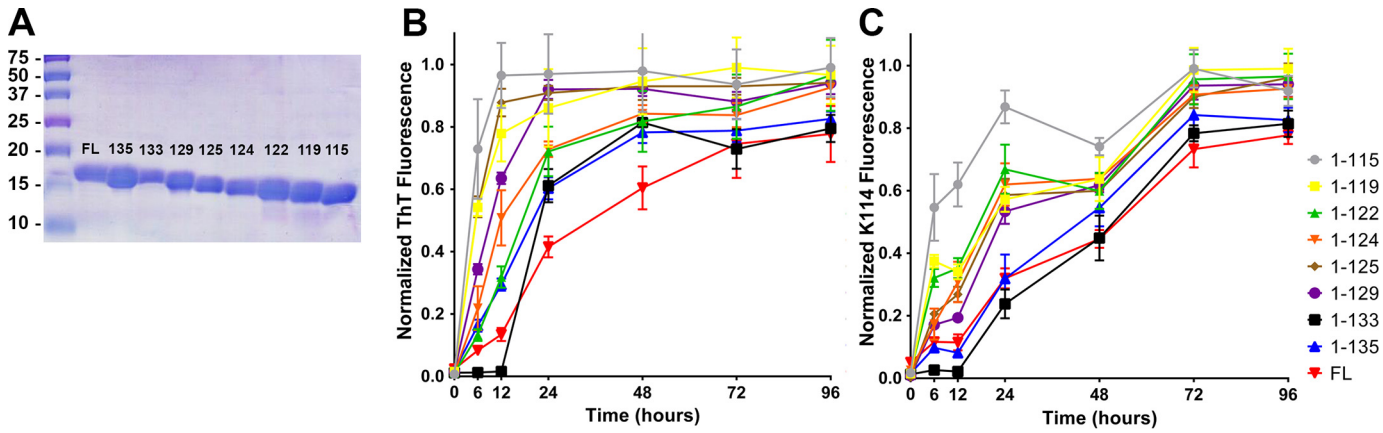

Figure 2. C-truncated αsyn aggregates rapidly and extensively *in vitro*. *A*, SDS-polyacrylamide gel showing purified C-truncated forms of αsyn. *B*, ThT fluorescence normalized to maximum fluorescent reading and final amount of insoluble αsyn at various time points ($n = 4$). Truncations 1–129 and shorter aggregate at an earlier time point compared with FL or C-truncated 1–133 and 1–135 αsyn. *Error bars*, S.D. *C*, K114 fluorescence normalized to maximum fluorescent reading and final amount of insoluble αsyn at various time points ($n = 4$). A similar trend to the ThT data is seen, where truncations 1–129 and shorter aggregate at a faster rate than FL αsyn.

Table 1

Statistical summary of *in vitro* aggregation rates

The normalized ThT fluorescence reading (Fig. 2*B*) for each C-truncated αsyn at each time point was compared with that of FL αsyn using two-way ANOVA and Dunnett's multiple-comparison test. 1–115, 1–119, and 1–125 αsyn aggregate most readily compared with FL, whereas the 1–133 and 1–135 αsyn truncations aggregate at a similar rate as FL. NS, no significance; *, $p \leq 0.05$; **, $p \leq 0.01$; ***, $p \leq 0.001$; ****, $p \leq 0.0001$.

	Two-way ANOVA multiple comparisons test compared with FL αsyn						
Truncation	0 h	6 h	12 h	24 h	48 h	72 h	96 h
1–115	NS	****	****	****	***	NS	NS
1–119	NS	****	****	****	**	*	NS
1–122	NS	NS	NS	**	NS	NS	NS
1–124	NS	NS	***	**	NS	NS	NS
1–125	NS	****	****	****	**	NS	NS
1–129	NS	*	****	****	*	NS	NS
1–133	NS	NS	NS	NS	NS	NS	NS
1–135	NS	NS	NS	NS	NS	NS	NS

the last time point. At 96 h of incubation, αsyn truncations 1–129 and shorter had a modest increase in aggregation extent compared with FL αsyn (Fig. S1, *A* and *B*), where 77.8 ± 2.8% of FL αsyn had become insoluble in PBS compared with 99.0 ± 0.9% for the 1–115 αsyn. Comparatively, 1–133 and 1–135 αsyn showed only a slight increase in the final amount of insoluble αsyn as determined from sedimentation analysis. These results demonstrate that *in vitro*, physiologic C-terminally truncated forms of αsyn aggregate more extensively and at a faster rate compared with FL αsyn, and the effect is generally accentuated with the increased extent of C-terminal truncation.

C-truncated αsyn forms amyloid fibrils assessed by transmission EM

FL αsyn is known to assemble *in vitro* into amyloid fibrils ranging between 5 and 12 nm in width (7, 37, 61–63). To assess whether physiologic C-truncated αsyn forms similar fibrils, FL and C-truncated αsyn proteins were individually incubated with shaking for 5 days followed by negative staining EM. All forms of C-truncated αsyn displayed fibril formation with a characteristic straight, unbranched appearance similar to FL αsyn (Fig. 3). Notably, fibrils composed of certain shorter C-truncations, such as 1–115, 1–119, 1–122, and 1–125 αsyn, tended to be shorter in length compared with those from FL αsyn, consistent with previous reports for other C-truncations (35, 37, 38). Additionally, the fibrils composed of the shorter proteins often formed dense "clumps" on the EM grid as opposed to a more even disbursement of fibrils, as is the case with fibrils composed of FL αsyn; this clustering is likely the result of less C-terminal charge, which otherwise would impair lateral packing of fibrils and has been reported for other C-truncations (35, 37–39). Observed widths (Fig. 3) were as follows: 1–115 = 8.52 ± 1.28, 1–119 = 10.62 ± 1.87, 1–122 = 13.98 ± 2.58, 1–124 = 15.31 ± 2.11, 1–125 = 15.35 ± 2.40, 1–129 = 15.11 ± 2.33, 1–133 = 12.77 ± 1.65, 1–135 = 13.88 ± 2.70, FL = 11.55 ± 2.39 nm. The fibril widths for the shorter proteins (*i.e.* 1–115 αsyn and 1–119 αsyn) were significantly less compared with FL αsyn (Fig. 3). This analysis demonstrates that all C-truncated forms of αsyn formed physiologically and commonly detected in LBs are capable of assembling into typical amyloid fibrils, albeit some with morphologic differences from FL αsyn.

C-truncated αsyn forms amyloid fibrils with differing proteolytic digestion profiles

Differential digestion products upon exposure to the proteases trypsin or proteinase K have been used previously to characterize differing strains of αsyn, as alternative fibril structures appear to undergo unique patterns of proteolytic digestion (64, 65). To ascertain unique digestion product profiles for each C-truncated form of αsyn, fibrils were assembled from each and incubated with two different concentrations of trypsin or proteinase K, followed by SDS-PAGE analysis (Fig. S2). Indeed, for trypsin and proteinase K digestion, resulting species varied in both size and number between the different C-truncated fibrils (Fig. S2). For C-truncations 1–125 and shorter, trypsin digestion results in two predominant bands, whereas three or more are evident for 1–129 and longer. For proteinase K digestion, only two major bands are seen for the 1–115, 1–122, and 1–124 fibrils, whereas multiple bands are evident for the others. This experiment indicates that structural differences may exist between these fibrils.

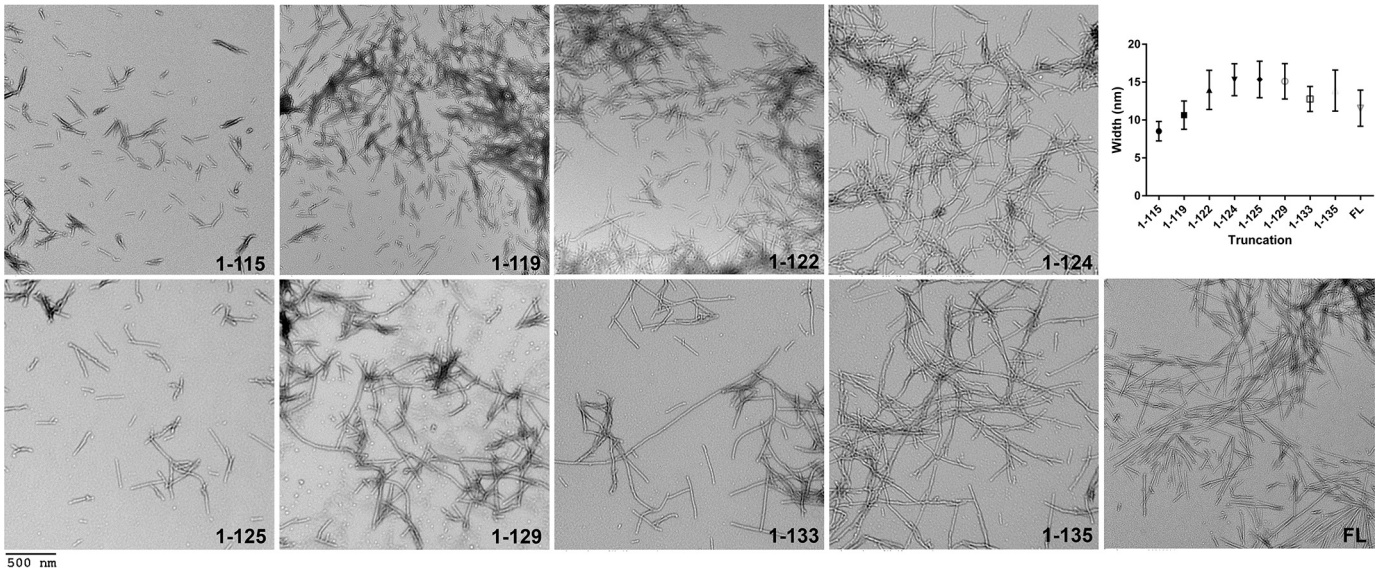

Figure 3. Electron micrographs of C-truncated αsyn fibrils. EM of all C-truncated and FL αsyn fibrils is shown; regions of sparser fibril population are shown to demonstrate individual fibril morphologies. The 1–115, 1–119, and 1–125 αsyn fibrils were noticeably shorter lengthwise compared with other fibrils. Fibril widths are displayed graphically, where average width eventually decreases for the most truncated species. *Error bars*, S.D. *Scale bar*, 500 nm.

Physiologic C-truncated forms of αsyn are extensively prone to prion-like aggregation in cell culture induced by preformed αsyn fibrillary seeds

Aggregation propensities between different αsyn missense mutants and other amyloid-forming proteins such as tau have been successfully studied in a cell culture model utilizing HEK293T cells, whereby cells are induced to express αsyn through calcium phosphate transfection, preformed αsyn fibrils are added, and resulting aggregation is assessed using detergent extraction, where monomeric, soluble and aggregated, insoluble αsyn are quantified via Western blotting (66–68). Using the same model with a similar experimental paradigm, our eight C-truncated forms of αsyn (Fig. 1) were expressed in HEK293T cells with or without treatment of preformed fibrils composed of 1 μM 21–140 αsyn, and the results were compared with cells expressing FL αsyn with the same treatment. The 21–140 αsyn fibrils induce pathology similarly to FL αsyn fibrils but are not detected by N-terminal antibody SNL4 (residues 2–12 in αsyn), allowing for detection of only expressed αsyn (66, 69–72). Cells were harvested in Triton X-100 fractionation buffer and the insoluble fibrillar species were isolated from soluble αsyn by ultracentrifugation. Without the addition of fibrillar αsyn seeds, intrinsically detergent-insoluble species were not observed for any of the C-truncated forms of αsyn investigated (Fig. 4*C*). Treatment with αsyn fibrillar seeds induced intracellular αsyn aggregation for FL αsyn and all eight C-truncated forms of αsyn (Fig. 4*A*). Compared with FL αsyn, 1–129 and shorter C-truncated forms of αsyn aggregated to a much greater extent (Fig. 4, *A* and *B*), whereas the truncations most like FL (1–133 and 1–135 αsyn) aggregated similarly to FL αsyn. A biphasic trend is also discernible, whereby truncation accelerates aggregation up until 1–124 αsyn, which corresponds to complete removal of the second acidic repeat in the C terminus of αsyn (Fig. 1); this trend of truncation increasing aggregation repeats itself from 1–124 to 1–115. Of note, a doublet band was observed in the insoluble portion for the 1–119 αsyn; it is unclear whether this is due to additional truncation or an alternative stable conformer. Overall, these findings demonstrate that the enhanced aggregation propensity of C-terminally truncated αsyn observed *in vitro* can be extended to a cellular milieu.

The seeded aggregation of these C-truncated forms of αsyn was further studied by utilizing immunofluorescence to directly visualize inclusions formed in HEK293T cells expressing C-truncated αsyn and treated with 21–140 αsyn fibrils, which are not detected by the antibodies used. SNL4 staining was ubiquitous for each truncation, suggesting similar levels of expression between them (Fig. 5). Additionally, SNL4 staining was seen throughout the cell body and processes, indicating that monomeric forms of αsyn were detected. Syn 506 is an antibody that preferentially detects aggregated αsyn in cultured cells (73), and Syn 506 detection was limited largely to rounded inclusions for all of the seeded cells but was minimal in unseeded cells (Fig. 5). In these experiments, more cells harbored Syn 506–positive inclusions when expressing C-truncated forms of αsyn that aggregated more extensively in biochemical studies, notably those 1–129 and shorter. Morphologically, inclusions were similar in size and shape between the different truncations. These findings suggest that the increased amount of seeded aggregation found for shorter C-truncated forms of αsyn is due to a higher probability of aggregation occurring in a given cell, leading to a higher number of Syn 506–positive cells.

The presence of C-truncated αsyn enhances aggregation of FL αsyn in vitro

Previous *in vitro* experiments have reported an enhancement of FL αsyn aggregation when co-fibrillized with some C-truncated αsyn monomers (35, 42, 43). To further assess this phenomenon using some of the distinct physiologic C-truncations,

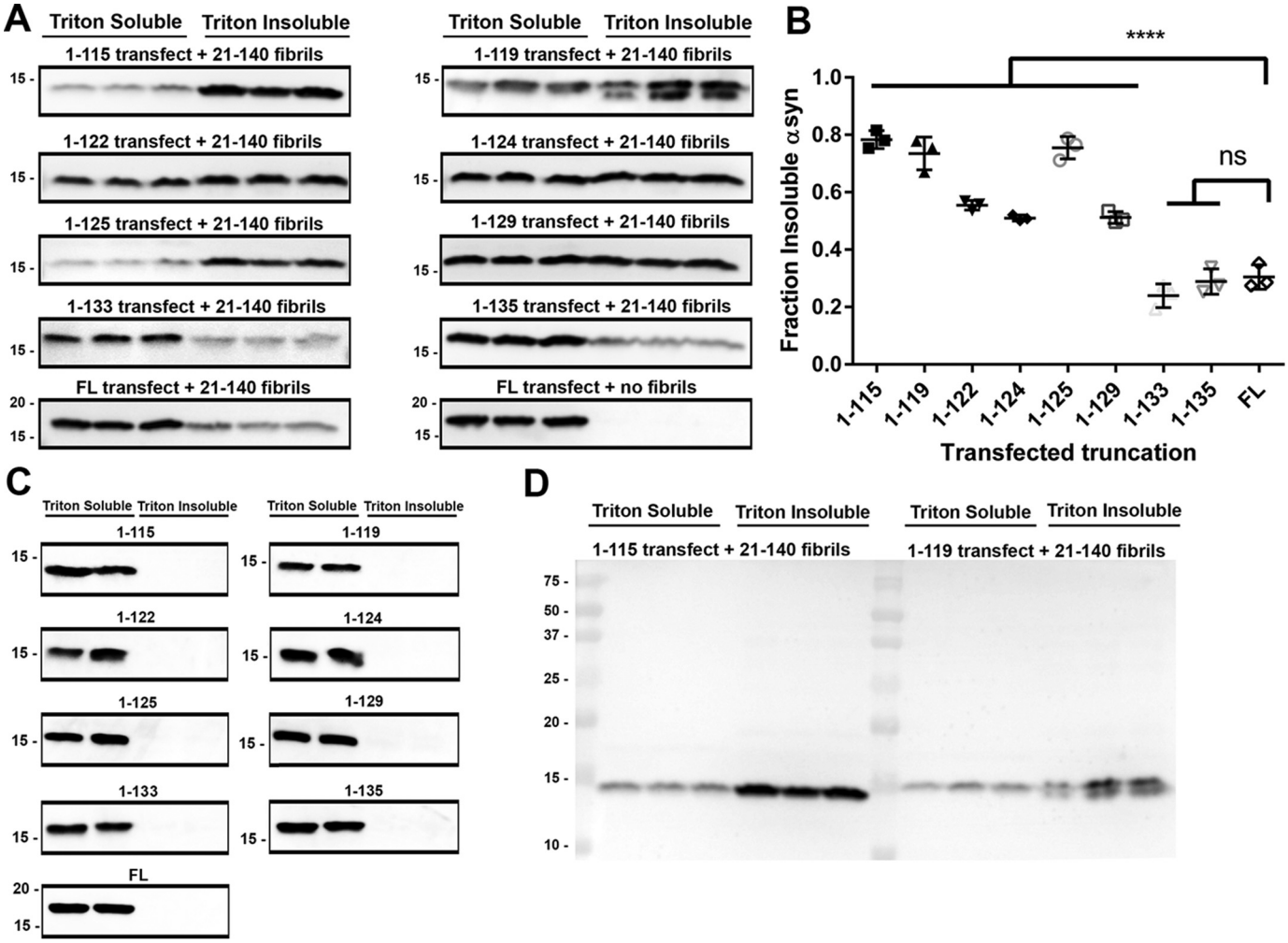

Figure 4. Enhanced aggregation of C-truncated αsyn in cultured cells with seeding. *A*, Western blots detecting the amount of Triton X-100–soluble and –insoluble αsyn from each cell culture sample ($n = 3$) that was transfected with the indicated αsyn truncation and treated with 1 μM 21–140 αsyn fibrils. SNL4 against residues 2–12 of αsyn was used, as it does not react with exogenous added fibrils. C-truncated αsyn aggregates to a greater extent than FL αsyn in this cellular model, and the effect is accentuated with increasing truncation. *B*, densitometric analysis of the blots in *A*; one-way ANOVA with Dunnett's test determined a large significant increase in the final extent of aggregation for C-terminal truncations 1–129 αsyn and shorter. *Error bars*, S.D. *ns*, no significance; ****, $p \leq 0.0001$. *C*, Western blot analysis of Triton X-100–soluble *versus* insoluble FL and C-truncated forms of αsyn expressed in HEK293T cells with no added fibrils. Antibody SNL4 against residues 2–12 of αsyn was used. No spontaneous aggregation was observed in this cell culture model. *D*, representative FL Western blotting (1–115 and 1–119 αsyn) of SNL4 demonstrating specificity for αsyn.

either 1–115, 1–125, 1–129, or 1–135 αsyn was diluted to 25 μM in PBS, and FL αsyn was additionally added to 25 μM ($n = 4$). Aggregation was then induced with shaking at 1050 rpm, 37 °C, and soluble *versus* insoluble FL αsyn was compared at time points of 0, 12, 24, 48, and 96 h using sedimentation analysis and densitometry (Fig. 6 and Table 2). For the 1–135/FL αsyn mixture, little if any aggregation occurred, as the 1–135 αsyn truncation appears to be highly similar to the FL protein, which does not appreciably aggregate at this concentration. Comparatively, with increasing extent of C-truncation from 1–129 and shorter, the FL protein is induced to aggregate at earlier time points. Most striking was the mixture of 1–115 with FL αsyn, where within 12 h, FL αsyn had aggregated to a greater extent than FL αsyn alone at 150 μM and 96 h (Fig. S1, *A* and *B*). Furthermore, FL αsyn and C-truncations appear to co-polymerize, as these became insoluble in a 1:1 ratio. These results demonstrate that physiologically C-truncated forms of αsyn can directly accelerate formation of FL αsyn fibrils through their robust tendency to aggregate.

Aggregation of FL αsyn is enhanced by the presence of C-truncated αsyn through the formation of mixed fibrils as visualized using immuno-EM

The results of the previous experiment were further investigated utilizing immuno-EM to determine the mechanism by which C-truncated αsyn was enhancing aggregation of FL αsyn. 21–140 and either 1–115 or 1–129 αsyn were co-aggregated in a 1:1 ratio to form fibrils that were immunolabeled with antibodies 4110 (residues 2–15 in αsyn) and 94-3A10 (residues 130–140 in αsyn). Control fibrils composed entirely of 21–140, 1–129, or FL αsyn at the same concentration as the co-aggregated fibrils were immunolabeled as well to demonstrate epitope specificity. Fibrils composed of either 21–140 + 1–115 αsyn or 21–140 + 1–129 αsyn were labeled with both antibodies 4110 and 94-3A10 when visualized using EM, demonstrating the presence of both the 21–140 αsyn and C-truncated αsyn within the same fibrils (Fig. 7*B*). The two antibodies were often binding tar-

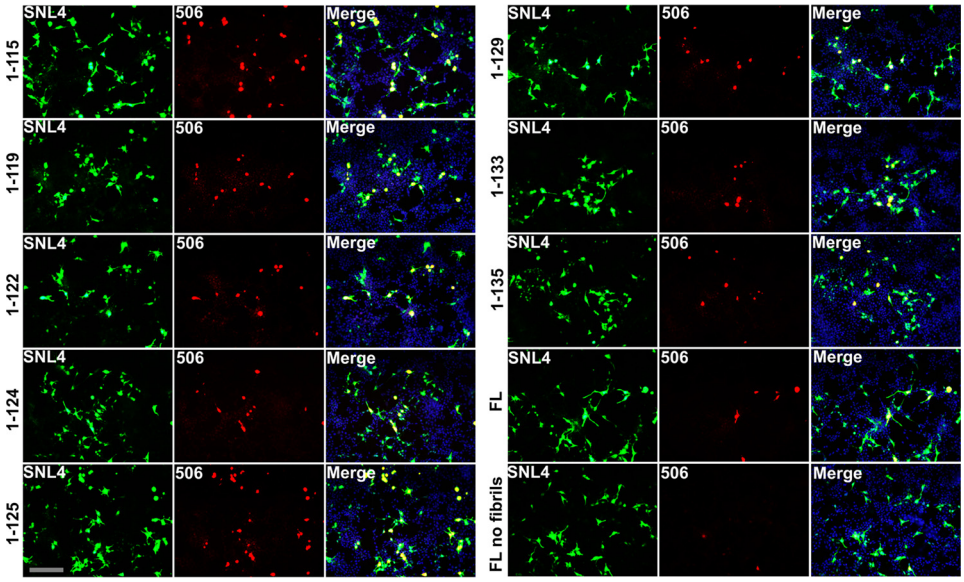

Figure 5. C-truncated αsyn forms extensive inclusions in cultured cells with αsyn seeding. Double immunofluorescence analysis shows the formation of αsyn inclusion pathology with αsyn antibody SNL4 (*green*) and aggregated αsyn-selective antibody Syn 506 (*red*) for HEK293T cells that were transfected with the indicated αsyn truncation and treated with 1 μM 21–140 αsyn fibrils. SNL4 and Syn 506 with epitopes against the N terminus of αsyn were used, as they do not react with exogenous added fibrils. C-truncated αsyn aggregates, as evidenced by Syn 506 staining, were found in a greater proportion of transfected cells than FL αsyn in this cellular model, and the trend is similar to that observed in biochemical fractionation experiments. Minimal Syn 506 staining is observed for cells transfected to express FL αsyn but without fibril treatment. Nuclei were counterstained with DAPI, and overlays are shown in the *right panels*. *Scale bar*, 100 μm.

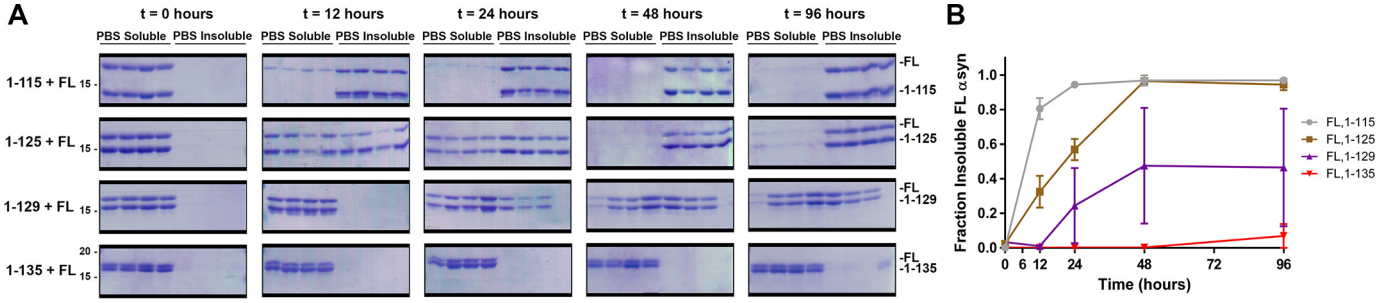

Figure 6. *In vitro* αsyn co-aggregation accelerates FL αsyn acceleration. *A*, Coomassie-stained SDS-polyacrylamide gels showing the amount of soluble and insoluble αsyn for C-truncated and FL αsyn co-fibrillized at 25 μM each over 96 h at 37 °C shaking ($n = 4$). *B*, densitometric analysis of the gels in *A*, quantifying the amount of FL αsyn aggregation at each time point for each co-fibrillization; more extensive C-truncation leads to quicker FL αsyn aggregation in a synergistic fashion. *Error bars*, S.D.

Table 2

Statistical summary of *in vitro* co-aggregation rates

The fraction of insoluble FL αsyn (Fig. 5*B*) for each C-truncated/FL αsyn co-fibrillization reaction at each time point was compared with that of FL/1–135 αsyn using two-way ANOVA and Dunnett's multiple-comparison test. The FL/1–115 co-fibrillization leads to almost complete aggregation of FL αsyn within 12 h, whereas little to no aggregation is seen for the FL/1–135 co-fibrillization at any time point. NS, no significance; *, $p \leq 0.05$; **, $p \leq 0.01$; ****, $p \leq 0.0001$.

	Two-way ANOVA multiple comparisons test compared with FL/1–135 αsyn				
Truncation	0 h	12 h	24 h	48 h	96 h
FL/1–115	NS	****	****	****	****
FL/1–125	NS	**	****	****	****
FL/1–129	NS	NS	*	****	****
FL/1–135	NS	NS	NS	NS	NS

gets within a few nanometers of each other on the same fibril, suggesting that the 21–140 and C-truncated forms of αsyn are each present throughout the mixed fibrils. FL αsyn fibrils were also detected by both antibodies, whereas 1–129 αsyn fibrils were only labeled by antibody 4110, and 21–140 αsyn fibrils were only detected by antibody 94-3A10. These findings indicate that aggregation-prone C-truncated forms of αsyn can induce FL αsyn to aggregate through the formation of mixed fibrils, as opposed to C-truncated αsyn independently forming fibrils that later seed FL aggregation.

The presence of C-truncated forms of αsyn enhances aggregation of FL αsyn in cell culture

To probe for any synergistic interactions in the aggregation process between FL and C-truncated forms of αsyn in cultured cells, HEK293T cells were co-transfected with plasmids expressing equal amounts of C-truncated and FL αsyn, followed by the addition of preformed 21–140 αsyn fibrils. Control transfections were performed where a pcDNA plasmid expressing FL αsyn was co-transfected with the empty pcDNA plasmid or a double amount of pcDNA plasmid expressing FL αsyn to examine whether a 2-fold alteration could significantly affect aggregation propensity, but similar levels of αsyn were observed regardless (Fig. 8, *A* and *B*). Co-expression of plasmids encoding 1–135 or 1–124 αsyn did not significantly influence the aggregation of FL αsyn (Fig. 8*B*). For αsyn C-truncations 1–133 and shorter, a trend

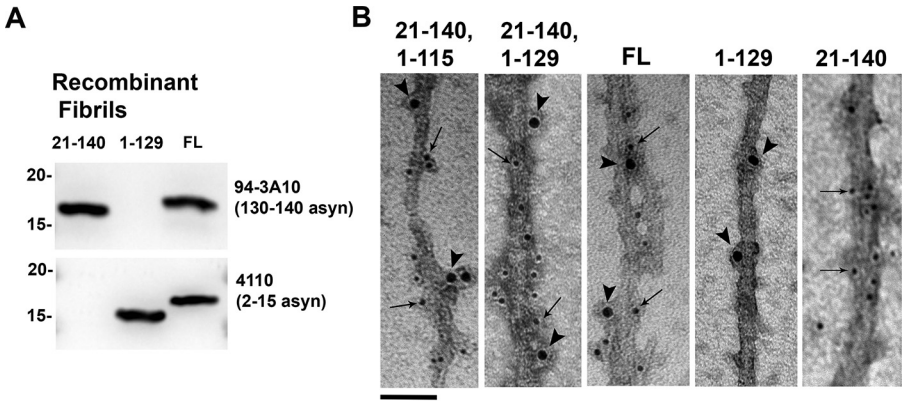

Figure 7. Electron micrographs of immunolabeled mixed fibrils composed of 21–140 and C-truncated αsyn. *A*, Western blots demonstrating epitope specificity of affinity-purified antibodies 4110 (2–15 αsyn) and 94-3A10 (130–140 αsyn) with lanes loaded with 200 ng of denatured recombinant fibrils composed of either 21–140, 1–129, or FL αsyn. Antibody 4110 reacts with FL and 1–129 αsyn, but not with 21–140 αsyn. Antibody 94-3A10 reacts with FL and 21–140 αsyn, but not with 1–129 αsyn. *B*, 21–140 and C-truncated αsyn were co-aggregated to form mixed fibrils, which were immunolabeled with antibodies 4110 and 94-3A10 and then detected by secondary antibodies conjugated to 10- or 6-nm gold nanoparticles, respectively. Fibrils composed of either 21–140 + 1–115 αsyn or 21–140 + 1–129 αsyn are reactive to both antibodies 4110 (*arrowheads*) and 94-3A10 (*arrows*), demonstrating the presence of both the 21–140 αsyn and C-truncated αsyn within the same fibrils. FL αsyn is labeled by both antibodies, 1–129 αsyn fibrils are only immunolabeled with antibody 4110, and 21–140 αsyn fibrils are only immunolabeled with antibody 94-3A10. *Scale bar*, 50 nm.

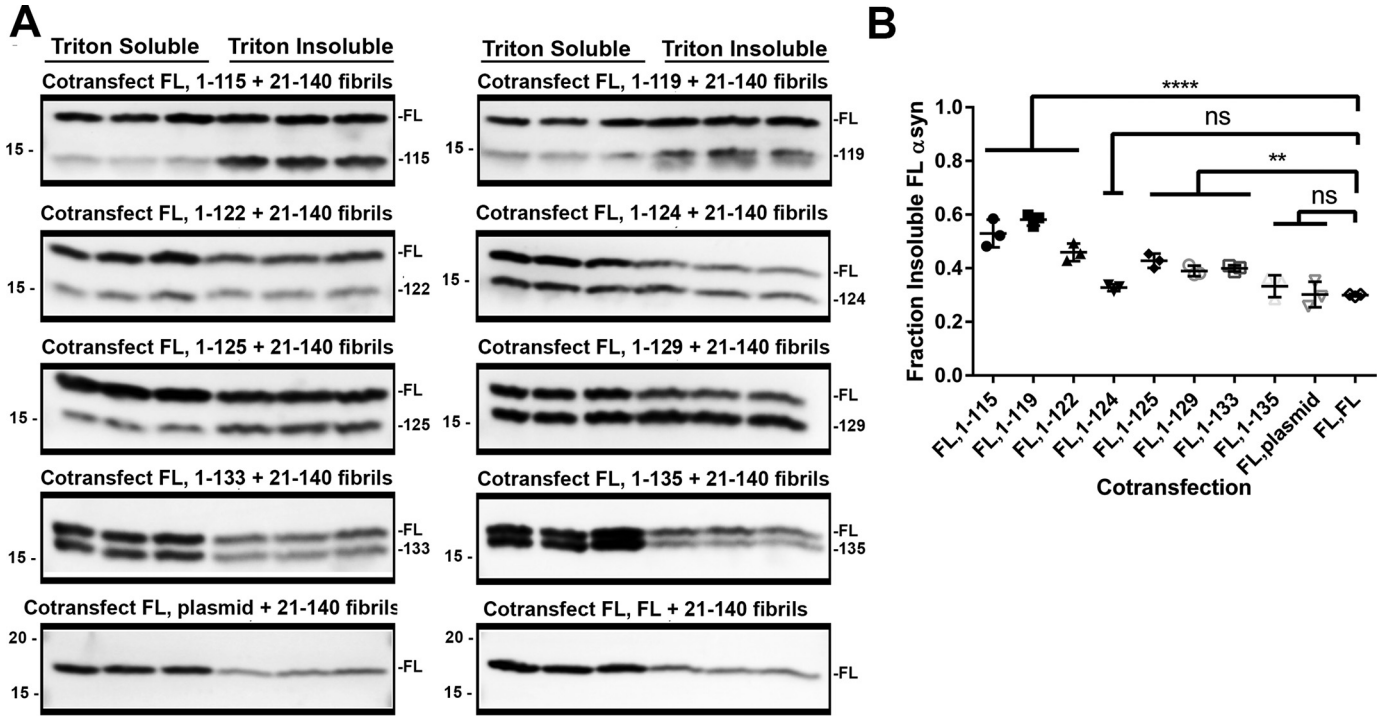

Figure 8. The presence of C-truncated αsyn potentiated FL αsyn aggregation in seeded cultured cells. *A*, Western blot analysis of Triton X-100–soluble and –insoluble αsyn from each cell culture sample co-transfected to express the indicated C-truncated αsyn and FL αsyn treated with 1 μM 21–140 αsyn fibrils. Antibody SNL4 against residues 2–12 of αsyn was used. C-truncated αsyn induces FL αsyn to aggregate more extensively compared with FL αsyn alone, and the effect is accentuated with increasing C-truncation. *B*, densitometric analysis of the blots in *A*; one-way ANOVA with Dunnett's test determined a significant increase in the final extent of FL αsyn aggregation for truncations 1–133 and shorter with the exception of 1–124. *Error bars*, S.D. *ns*, no significance; **, $p \leq 0.01$; ****, $p \leq 0.0001$.

is observed whereby co-transfection for plasmids encoding increasingly C-truncated αsyn leads to a greater proportion of aggregated, insoluble FL αsyn (Fig. 8*B*). Aggregation of FL αsyn, where cells were transfected with plasmid encoding FL αsyn + empty plasmid or double the amount of FL αsyn plasmid, was 30.0 ± 3.8 and 29.9 ± 0.4%, respectively. The amount of FL αsyn aggregation was increased to 53.0 ± 4.2 and 58.1 ± 1.8% when co-transfected with plasmids encoding the 1–115 αsyn and 1–119 αsyn. This trend of a synergistic increase in FL aggregation with further C-terminal truncation is broken by the 1–124 αsyn truncation, corresponding to the removal of one entire acidic C-terminal repeat (Fig. 1). These results suggest that a pathologic role for C-truncated αsyn may not just be limited to cellular dysfunction resulting from its own aggregation, but in fact αsyn C-truncations that are primed to aggregate may assist in initiating FL αsyn fibrillization. Furthermore, this synergistic aggregation is mechanistically explained by formation of fibrils containing both C-truncated and FL αsyn, as evidenced by *in vitro* experiments and immuno-EM.

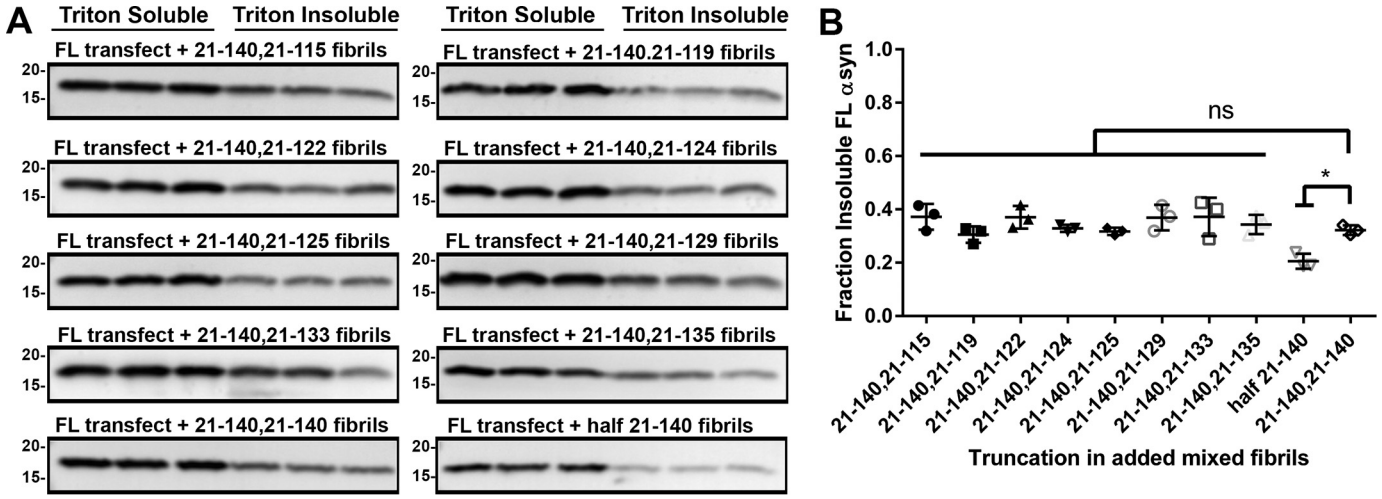

Figure 9. Fibrils composed of mixed C-terminally truncated αsyn and intact C terminus αsyn are potent at inducing FL αsyn aggregation in cultured cells. *A*, Western blot analysis of the amount of Triton X-100–soluble and –insoluble FL αsyn from each cell culture sample transfected with FL αsyn and treated with 1 μM mixed 21–140 αsyn and the respective C-truncated αsyn fibrils generated by incubating 21–140 αsyn with C-truncated 21–140 αsyn in a 1:1 ratio. Antibody SNL4 against residues 2–12 of αsyn was used. *B*, densitometric analysis of the blots in *A*; one-way ANOVA with Dunnett's test determined equal seeding ability of the mixed fibrils compared with FL αsyn; a small but significant decrease in aggregation is seen when a half-dose of 21–140 αsyn fibrils is used. *Error bars*, S.D. *ns*, no significance; *, $p \leq 0.05$.

αsyn fibrils potentiated by C-truncated αsyn demonstrate potent activity as prion-like seeds in HEK293T cells

Results of the previous experiments show that αsyn fibrils form much more readily when both C-truncated and FL αsyn are present compared with FL αsyn alone. Furthermore, these fibrils contain both C-truncated and FL αsyn when both are available in aggregation conditions. To determine the ability of these mixed C-truncated/FL αsyn fibrils to seed FL αsyn aggregation in cultured cells, the eight C-truncated forms of αsyn (Fig. 1) but further missing N-terminal residues 1–20 (to allow for detection of only the cellularly expressed αsyn using antibody SNL4) were co-fibrillized with 21–140 αsyn in a 1:1 ratio and added at 1 μM to HEK293T cells transfected to express FL αsyn (Fig. 9, *A* and *B*). Control experiments were performed where 21–140 αsyn fibrils alone were added at either 0.5 or 1 μM for comparison (Fig. 9, *A* and *B*). All of the mixed fibrils composed of FL and C-truncated forms of αsyn were capable of inducing substantial but similar FL αsyn aggregation compared with fibrils composed of only FL αsyn. A small but significant decrease in aggregation is seen when only 21–140 αsyn fibrils are used but at half the concentration, indicating that the presence of C-truncated αsyn can substitute for FL αsyn in the fibril structure while maintaining pathogenicity (Fig. 9*B*). These findings demonstrate that mixed fibrils containing C-truncated and FL αsyn fibrils that form at an accelerated rate are equally potent in their prion-like ability to propagate αsyn aggregation compared with FL αsyn fibrils.

Fibrils composed entirely of C-truncated αsyn cross-seed FL αsyn less efficiently in cell culture, suggesting structural incompatibility

Recent evidence suggests that fibrils formed entirely of C-truncated αsyn can be conformationally distinct (41), as is the case with fibrils composed of E46K αsyn or proposed alternative strains of αsyn (74–78); these alternative αsyn fibrils often have inefficient cross-seeding of FL αsyn, which is seen with added E46K fibrils to FL αsyn (74, 79). To investigate the ability of fibrils composed entirely of C-truncated forms of αsyn to template polymerization of FL αsyn, HEK293T cells were transfected with the plasmid expressing FL αsyn and treated with 1 μM preformed fibrils individually composed of each of the eight truncations used in this study or the 21–140 αsyn control. The antibody 94-3A10 that requires residues 135–140 in αsyn does not detect any C-truncations used and was used to detect FL αsyn expressed in the cells (80). Most of the fibrils composed solely of C-truncated forms of αsyn seeded FL αsyn less efficiently than 21–140 αsyn, and 1–122 and 1–124 αsyn fibrils induced little if any FL αsyn aggregation (Fig. 10, *A* and *B*). These results indicate that fibrils composed entirely of C-truncated αsyn are structurally distinct and consequently less efficient in seeding FL αsyn, demonstrating that the C terminus of αsyn has an active role in determining fibril structure.

The 5G9 mAb preferentially detects aggregated mouse αsyn

To facilitate identification of aggregated mouse αsyn in neuronal-glial culture, a novel mAb raised against residues 117–129 of mouse αsyn was generated. Specificity for mouse αsyn with no cross-reactivity for human αsyn was demonstrated using both recombinant protein and HEK293T cell culture lysate, where cells were transfected to express either human or mouse αsyn (Fig. S3*A*). Furthermore, using tissue from C3HBL/6 mice intrastriatally injected with mouse αsyn fibrils, which demonstrate αsyn inclusions in the ipsilateral entorhinal cortex (81), the 5G9 antibody was shown to preferentially bind to aggregated mouse αsyn, paralleling staining for $pSer^{129}$ (Fig. S3*B*). Additionally, there was no 5G9 staining in the contralateral entorhinal cortex, where pathology was not present in the mice used, demonstrating that this antibody is conformationally specific for mouse αsyn in an aggregated state. This experiment provides a useful tool for detection of aggregated mouse αsyn induced to form from human αsyn fibrils.

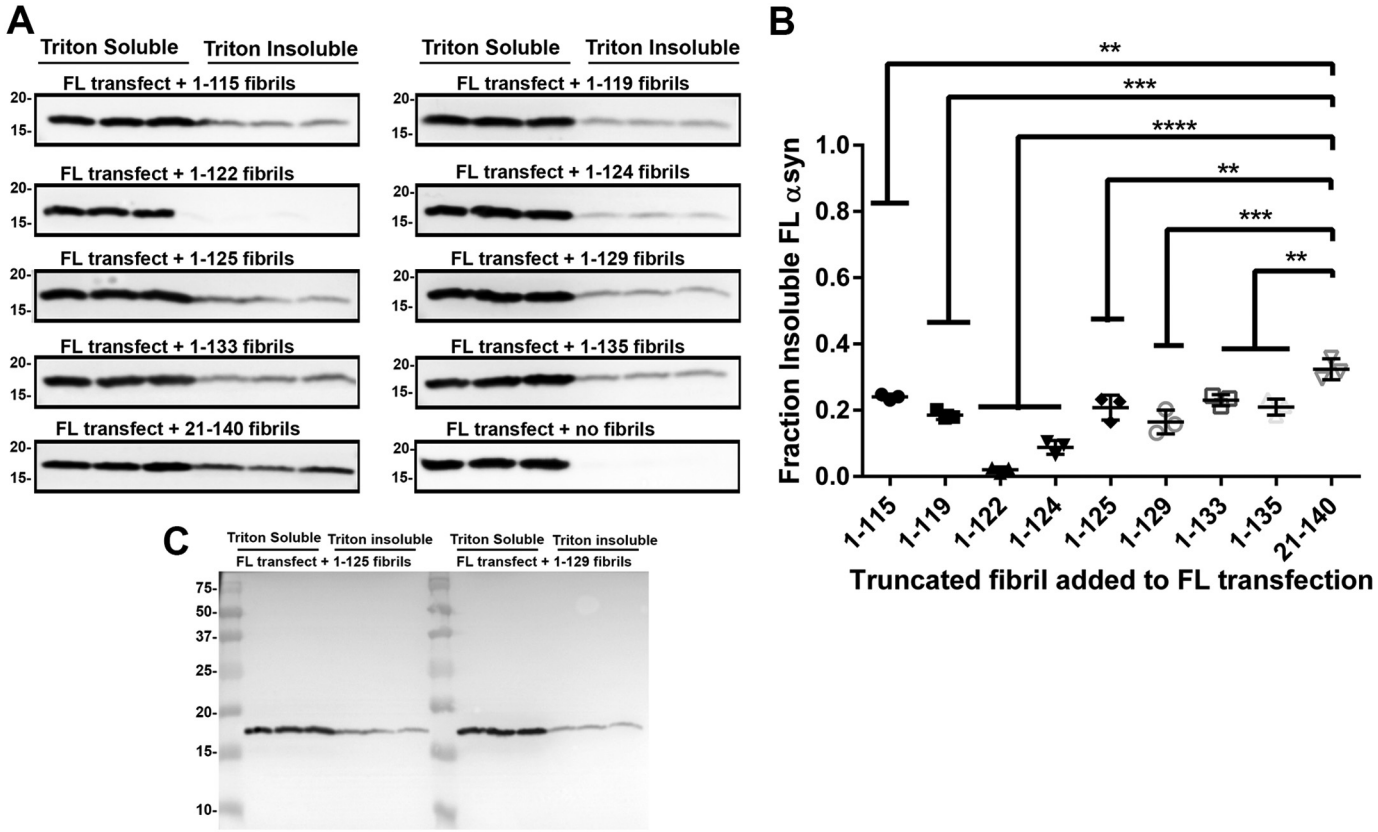

Figure 10. αsyn fibrils formed solely of human C-truncated αsyn are less efficient at seeding FL αsyn aggregation in cultured cells. *A*, Western blot analysis of Triton X-100–soluble and –insoluble FL αsyn from each cell culture sample ($n = 3$) transfected with FL αsyn and treated with 1 μM C-truncated αsyn fibrils. Antibody 94-3A10 against residues 130–140 of αsyn was used for all Western blots except for the 21–140 αsyn fibrils to FL αsyn, which was analyzed with antibody SNL4 against residues 2–12. Fibrils composed solely of C-truncated αsyn are less efficient at inducing αsyn-seeded aggregation compared with 21–140 αsyn fibrils. *B*, densitometric analysis of the blots in *A*; one-way ANOVA with Dunnett's test determined lessened seeding ability of C-truncated αsyn fibrils compared with 21–140 αsyn. *Error bars*, S.D. **, $p \leq 0.01$; ***, $p \leq 0.001$; ****, $p \leq 0.0001$. *C*, representative FL Western blotting (added 1–125 and 1–129 αsyn fibrils) of 94-3A10, demonstrating specificity for αsyn.

Fibrils composed entirely of C-truncated human αsyn seed mouse FL αsyn inefficiently in neuronal-glial culture, suggesting structural incompatibility

To confirm the observation that fibrils composed entirely of C-truncated αsyn do not seed FL αsyn efficiently, primary neuronal-glial cultures isolated from the cortex of embryonic day 16 (E16) C3HBL/6 mice were treated for 10 days with 1.5 μM C-truncated fibrils composed entirely of either 1–115, 1–125, 1–129, or FL αsyn (Fig. 11*A*). Indeed, the pure C-truncated αsyn fibrils resulted in little to no FL αsyn aggregation, whereas FL αsyn fibrils induced 18.3 ± 5.3% aggregation (Fig. 11*B*). These findings for seeding with FL and C-truncated αsyn fibrils were confirmed by immunofluorescence analysis staining for αsyn inclusion pathology using $pSer^{129}$ or 5G9 antibodies (Fig. 12).

FL αsyn fibrils potentiated and copolymerized with C-truncated αsyn demonstrate robust activity as prion-like seeds in neuronal-glial culture

To investigate the potential for αsyn fibrils composed of both FL and C-truncated αsyn to induce pathology in neuronal cells, primary E16 neuronal-glial cultures were seeded with these mixed fibrils. 1–115, 1–125, or 1–129 αsyn truncations were individually co-fibrillized with FL αsyn and used to treat the neuronal cultures at 1.5 μM for 10 days. Compared with fibrils composed solely of the C-truncated αsyn proteins that induced little to no aggregation of the endogenous mouse αsyn, the addition of the mixed fibrils led to an equal or even slightly greater amount of insoluble mouse αsyn compared with FL αsyn fibrils (Fig. 11). These findings were confirmed by immunofluorescence analysis with anti-$pSer^{129}$ and 5G9 staining (Fig. 12).

Discussion

In these studies, we systematically examined the aggregation properties of common and naturally occurring C-terminal truncations of αsyn that were previously identified to form when either monomeric or fibrillar αsyn are introduced to cells; most of these truncations have additionally been purified from LB inclusions in human disease (32, 34, 42–48, 82). Our data suggest that the formation of these C-truncated species may contribute to initiating αsyn aggregation. Mechanistically, the C terminus of αsyn is seemingly engineered to inhibit aggregation due to several factors. First, the acidic residues in the C terminus promote a disordered structure and maintain protein solubility (83, 84); fusion of the C terminus to other proteins is even sufficient to render them solubilized and stable against heat-induced precipitation (85, 86). Second, the C terminus has

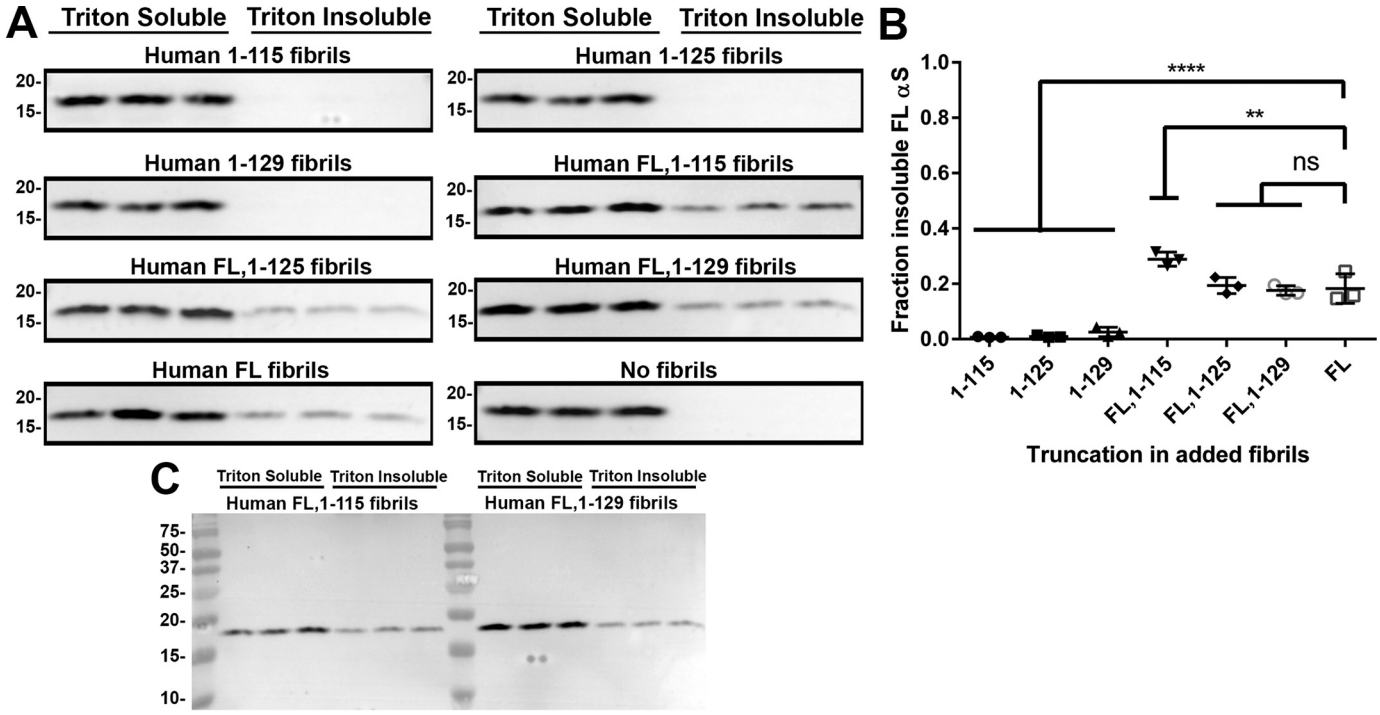

Figure 11. Fibrils composed of mixed human FL and C-terminally truncated αsyn induce FL αsyn aggregation in neuronal-glial cultures. *A*, Western blot analysis detecting Triton X-100–soluble and –insoluble mouse FL αsyn from E16 neuronal-glial cultures ($n = 3$) treated with a 1.5 μM concentration of either C-truncated αsyn fibrils generated only from a single C-truncated form of human αsyn or in a 1:1 ratio of each C-truncated αsyn with FL αsyn. Antibody D37A6 specific for mouse αsyn was used for all Western blots. Seeds composed only of C-truncated human αsyn are not efficient at inducing mouse αsyn aggregation compared with FL human αsyn fibrils. Mixed C-truncated/FL αsyn fibrils were largely equivalent in seeding potential compared with FL αsyn fibrils. *B*, densitometric analysis of the blots in *A*; one-way ANOVA with Dunnett's test determined lessened seeding ability of fibrils composed of only C-truncated αsyn compared with those assembled from FL αsyn or mixed FL/C-truncated αsyn. *Error bars*, S.D. *ns*, no significance; **, $p \leq 0.01$; ****, $p \leq 0.0001$. *C*, representative FL Western blotting (FL,1–115 and FL,1–129 αsyn) of D37A6 demonstrating specificity for mouse αsyn.

autochaperoning abilities, whereby it establishes contacts with the hydrophobic NAC region to shield it from pathologic aggregation-inducing interactions (38, 87–91). Lastly, the C terminus is the most proline-rich region in αsyn, with 5 proline residues known to be unfavorable to β-sheet formation (83, 92). Additionally, these C-terminal prolines form a Nedd4 ubiquitin ligase consensus sequence that promotes degradation of αsyn (93). All of these protective features are lost upon C-terminal truncation, and consequently C-terminal truncation of αsyn has been repeatedly shown to promote *in vitro* fibril formation (35, 36, 38, 41–43, 94). Comparatively, N-terminal truncation has been shown to either not affect aggregation or mildly decrease it (95–97); this is expected due to the inconsequential changes in basic biochemical properties, such as protein pI and hydrophobicity, that are induced when the amphipathic N terminus is truncated (Fig. S4).

In vitro aggregation assays of these physiologic C-truncated forms of αsyn demonstrated that C-terminal truncation enhances spontaneous fibril formation, with more extensive removal of residues generally corresponding to further acceleration of the polymerization process. Furthermore, for the 1–129 and shorter C-truncations there is an increase in the final extent of aggregation, suggesting that the critical concentration of monomers for fibril formation may be lower for the more extensive C-truncated species compared with FL αsyn (17). Analyzing polymers of C-truncated αsyn using EM, the clearest morphologic difference between them and FL fibrils is a decrease in observed fibril length. In the context of nonseeded aggregation in which these fibrils were generated, this finding is likely because initial spontaneous aggregate formation for these C-truncated proteins occurred with high frequency, leading to an increased number of shorter fibrils as the monomer/fibril ratio decreased rapidly, not allowing individual fibrils to excessively elongate. Comparatively, the FL protein with a lesser propensity to spontaneously aggregate would be expected to have rarer fibril-forming events, allowing the initially formed fibrils to polymerize further before monomers are sufficiently depleted to halt fibrillization. This decrease in length with C-truncation has been noted previously *in vitro* for other forms of C-truncated αsyn (35, 37, 38), but never for these physiologic truncations. From these experiments, it is clear that physiologic C-truncation of αsyn accelerates both the extent and rate of fibril formation, and the mechanism for this is likely due to a lower energy barrier for spontaneous initial aggregation, leading to the shorter fibrils observed in EM.

From initial cell culture experiments, it is evident that physiologic C-truncated αsyn aggregates more extensively than FL αsyn even in a cellular environment, but in the time frame of studies in HEK293T cells, this process requires seeding. Intriguingly, the truncations most similar to FL aggregate to a similar degree, but C-truncations that are 1–129 or shorter demonstrate a much greater amount of insoluble, aggregated αsyn, which follows the trends in aggregation extent and speed determined *in vitro*. This accelerated aggregation seen when C-truncated forms of αsyn are seeded with 21–140 αsyn fibrils is presumably due to elongation of the initial seed fibrils from

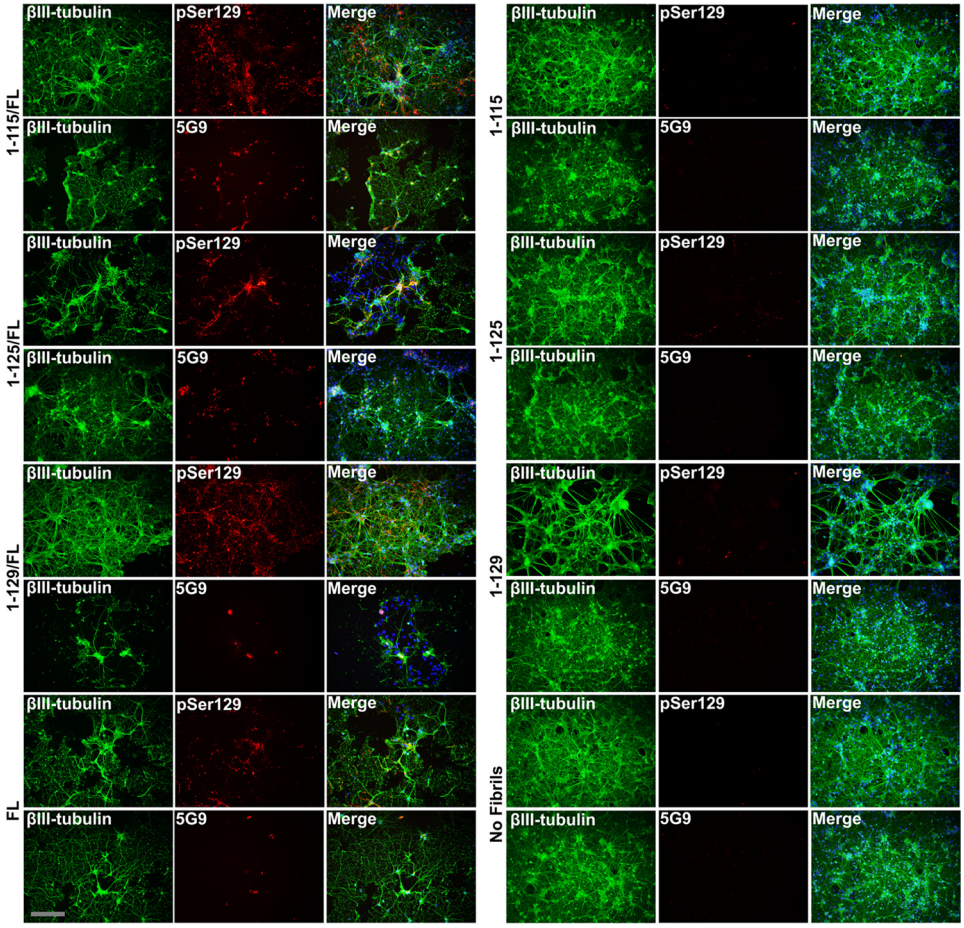

Figure 12. Mixed human C-truncated/FL αsyn fibrils induce pathologic inclusions in neuronal-glial culture. Shown is double immunofluorescence analysis demonstrating the formation of αsyn inclusion pathology with pSer^{129} αsyn antibody EP1536Y or aggregated mouse αsyn-selective antibody 5G9 double-labeled with βIII-tubulin neuronal specific antibodies. E16 neuronal-glial cultures were treated with 1.5 μM αsyn fibrils composed entirely of C-truncated forms of αsyn or in a 1:1 ratio of each C-truncated form of αsyn with FL αsyn as indicated. Mixed C-truncated/FL human αsyn fibrils induced αsyn inclusion pathology in neurons (*left*), whereas fibrils composed entirely of C-truncated αsyn did not (*right*). *Scale bar*, 100 μm.

these monomers with more exposed NAC regions and less negative repulsion due to loss of acidic C-terminal residues. Cumulatively, the *in vitro* and cell culture experiments revealed that C-truncated αsyn is primed to aggregate, which may be crucial in initial disease pathogenesis. Also, αsyn fibrils are known to be trafficked to lysosomes in neurons (21, 98), where these truncations are likely formed (22, 30–34), and may play a role in initial fibril-induced propagation of pathology, as the C-truncated forms of αsyn are much more readily induced to aggregate compared with FL αsyn.

Previous *in vitro* experiments have reported an enhancement of αsyn aggregation when co-fibrillized with C-truncated αsyn monomers (35, 42, 43). Herein, we demonstrated that this phenomenon occurs with physiologic C-truncations of αsyn and at low concentrations, close to physiologic 3 μM (17), where FL αsyn would otherwise not aggregate *in vitro*. It is demonstrated that co-incubation of FL αsyn with 1–115 or 1–125 αsyn increased not only the rate of FL αsyn aggregation but also the final total extent, where nearly all of the FL αsyn became insoluble under these conditions. These results demonstrate that C-truncated αsyn may induce initial FL αsyn fibril formation when it otherwise would not occur, and the mechanism for this appears to be mixed C-truncated/FL αsyn fibril formation, as both FL and C-truncated forms of αsyn became insoluble in equal proportions. The formation of the proposed mixed fibrils was shown by immuno-EM, where both C-truncated forms of αsyn and 21–140 αsyn were detected throughout fibrils when co-assembled. In cultured cells, co-transfection to express FL αsyn with the more extensively C-truncated αsyn species led to an almost doubling of FL αsyn aggregation in the presence of 21–140 seed fibrils. Thus, C-truncated forms of αsyn may be pathologically relevant not only due to their robust aggregation propensity and ability to be seeded by αsyn fibrils, but also in synergistically accelerating seeded or unseeded aggregation of FL αsyn. The cell culture results in the context of seeded aggregation could be explained by the aggregation-prone C-truncated monomers rapidly elongating the seed fibrils, promoting their eventual fracturing into smaller fibrils (containing both FL and C-truncated αsyn) that are known to readily seed further templating (17, 19, 99, 100). Our cumulative results suggest that aggregation-prone forms of C-truncated αsyn may play a role in initial inclusion formation as they potentiate FL αsyn aggregation through formation of mixed fibrils. Furthermore, the resulting mixed fibrils composed of both C-truncated and FL αsyn demonstrated a potent ability to propagate further αsyn aggregation in both HEK293T cells and primary neuronal-glial cultures.

αsyn fibrils composed partially of C-truncated αsyn along with FL αsyn are probabilistically more likely to form than fibrils composed entirely of C-truncated αsyn; however, the seeding ability of pure C-truncated αsyn fibrils was investigated to understand the necessary role of the C terminus in fibril structure and pathogenicity. Indeed, these pure C-truncated αsyn fibrils were less efficient in their induction of αsyn aggregation, suggesting structural incompatibility between the seeds and endogenous αsyn. These findings are consistent with previous *in vitro* findings and other reports in cultured cells, where 1–120 αsyn fibrils or 1–99 αsyn fibrils when added to cells also yield lower templating of FL αsyn (41, 64, 66, 101, 102). However, a study utilizing C-truncated fibrils formed from proteolytic digestion noted either equal or superior seeding compared with FL αsyn fibrils (31), which is presumably due to mixed C-truncation/FL αsyn fibril formation, as it is unlikely that all αsyn within a fibril becomes C-truncated. The conflicting results of these previous studies are explained by our own observations, where any pathologic role of C-truncated αsyn is likely mediated through synergistic aggregation with FL αsyn and the appearance of mixed C-truncated/FL αsyn fibrils but not through formation of only C-truncated fibrils. This notion agrees with a recent study where it was found that fibrils composed entirely of nonphysiologic C-truncated αsyn may lead to structural incompatibility with FL αsyn in cultured cells and in seeding of pathology in mouse models (102).

In the context of prion-like conformational templating, it seems paradoxical that C-truncated αsyn readily aggregates in the presence of FL αsyn fibrils, but, conversely, the addition of pure C-truncated αsyn fibrils to FL αsyn leads to lessened fibril formation. All truncations used in this study have identical fibril core–forming residues from ~30 to 102, which includes the NAC region implicated in prion-like conformational templating (61, 63, 103–105), suggesting that C-truncated αsyn fibrils should still induce FL αsyn fibril formation. These results might be explained by the recently discovered alternative structure assumed by fibrils composed entirely of C-truncated αsyn (41). In a typical αsyn fibril, the highly charged and bulky disordered C termini must be maximally separated between αsyn subunits, which is achieved with a less compact fibril structure. Comparatively, fibrils composed of C-truncated αsyn can assume a more highly twisted and compact conformation that is not amenable to the addition of FL αsyn, explaining the inefficient cross-seeding (41). Under this model, C-truncated αsyn would readily add onto FL fibrils; however, the addition of FL αsyn to the more compact C-truncated fibrils would be less efficient, as unfavorable C-terminal repulsions would occur. This model is consistent with the data presented here and suggests that the C terminus and other common post-translational modifications may intrinsically alter fibril structure and resulting prion-like conformational templating. Differing proteolytic digestion profiles of C-truncated αsyn fibrils corroborate the possibility that C-truncation has a profound effect on fibril structure that may lead to cross-seeding differences. Alterations in the αsyn fibril ultrastructure may underlie prion-like strain differences and constitute C-truncated fibrils as alternative strains themselves.

In summary, these results suggest that physiologically C-truncated forms of αsyn may be pathologic due to their strong aggregation propensity, their potentiation of FL αsyn aggregation, and the ability of resulting mixed C-truncated/FL αsyn fibrils to propagate further FL αsyn aggregation. It is conceivable that the processing of αsyn to form C-truncated αsyn in lysosomes may facilitate initial αsyn fibril formation through the mechanisms studied herein, resulting in fibrils capable of mediating the pathologic progression of LB pathology through subsequent prion-like spread. These experiments add to a growing collection of data supporting a lysosome-centered explanation of synucleinopathies, whereby pathologic impairment of proteostasis may be an important contributor to disease.

Experimental procedures

Antibodies

Anti-phosphorylated Ser^{129} ($pSer^{129}$) αsyn rabbit mAb EP1536Y was obtained from Abcam (Cambridge, MA). SNL-4 is a rabbit polyclonal antibody raised against residues 2–12 of αsyn (72). 4110 is a rabbit antibody raised against a peptide corresponding to residues 2–15 in human αsyn with an added cysteine at the N terminus (CDVFMKGLSKAKEGV) for conjugation to maleimide-activated mariculture keyhold limpet hemocyanin (Thermo Scientific, Waltham, MA) as a service provided by GenScript (Piscataway, NJ). Antibody 4110 was further affinity-purified using recombinant FL human αsyn conjugated to Affi-Gel 15 beads from Bio-Rad. 94-3A10 is a mouse mAb specific for the extreme C-terminal 130–140 residues of αsyn (80). 94-3A10 was further affinity-purified using a Protein G chromatography cartridge from Thermo Fisher Scientific. D37A6 is a rabbit mAb specific for mouse αsyn that was purchased from Cell Signaling (Danvers, MA). The Tuj-1 mouse mAb for neuronal specific βIII tubulin was purchased from R&D Systems (Minneapolis, MN). Neuronal specific rabbit anti-βIII tubulin antibody (T2200) was obtained from Sigma-Aldrich. Syn 506 is a mouse mAb to residues 2–12 of αsyn that preferentially binds aggregated αsyn (73, 106).

Expression and purification of recombinant αsyn proteins

Recombinant FL human αsyn along with N-terminally truncated 21–140 human αsyn were expressed from the pRK172 plasmid containing the cDNA for the *SNCA* gene as described previously (61, 67). Additional stop codons were introduced in these two constructs through QuikChange site-directed mutagenesis (Agilent Technologies, Santa Clara, CA) using mutant-specific oligonucleotides to generate expression plasmids yielding eight different C-terminally truncated αsyn proteins (Fig. 1) (66). All mutations and the absence of errors throughout the entire length of the αsyn cDNA were confirmed by Sanger sequencing. FL (residues 1–140), 1–129, 1–133, 1–135, 21–140, 21–129, 21–133, and 21–135 αsyn were expressed in *Escherichia coli* BL21 (DE3) and purified as described previously, utilizing size-exclusion and Mono Q anion-exchange chromatography (61). For the shorter αsyn truncations, which are 1–115, 1–119, 1–122, 1–124, 1–125, 21–115, 21–119, 21–122, 21–124, and 21–125 αsyn, following expression in *E. coli* BL21 (DE3), proteins were purified with a

modified procedure in which the Mono Q anion-exchange elution buffers were prepared at pH 9 to account for increasing pI in these truncated proteins. All recombinant proteins were diluted in pH 7.4 sterile PBS (Invitrogen), and concentrations were determined using the bicinchoninic acid assay (Pierce) with BSA as the standard.

In vitro aggregation of C-truncated αsyn

For *in vitro* aggregation comparisons, FL and C-truncated αsyn proteins were diluted to 150 μM in sterile PBS (Invitrogen) and assembled into amyloid fibrils with continuous shaking at 1050 rpm, 37 °C, for 0, 6, 12, 24, 48, 72, and 96 h with four replicates per protein at each time point. Amyloid formation for each tube ($n = 4$) was assessed by K114 and ThT fluorometry as described previously (60). Additionally, insoluble polymer formation at the final time point (40 μl of solution) was measured by centrifugation at 100,000 × *g* for 30 min in PBS. SDS-sample buffer was added to the separated pellets and supernatants to the same final concentration (10 mM Tris, pH 6.8, 1 mM EDTA, 40 mM DTT, 0.005% bromphenol blue, 0.0025% pyronin yellow, 1% SDS, 10% sucrose). Supernatant and pellet samples at the same volume were boiled for 10 min, and equal volumes from each fraction were resolved in SDS-PAGE using 15% polyacrylamide gels. Gels were stained with Coomassie Blue R-250 to visualize protein and destained in 25% isopropyl alcohol, 10% acetic acid; densitometric analysis of stained αsyn protein bands was conducted using the ImageJ program to quantify the fraction of insoluble αsyn for each sample.

In vitro co-aggregation of C-truncated and FL αsyn

To assay any enhancement of FL αsyn aggregation when C-truncated αsyn is present *in vitro*, 25 μM FL αsyn was mixed with a 25 μM concentration of either the 1–115, 1–125, 1–129, or 1–135 αsyn proteins and assembled into fibrils identically to the *in vitro* aggregation comparison experiment. At times of 0, 12, 24, 48, 72, and 96 h, 40 μl of solution was withdrawn from each tube and analyzed through insolubility analysis as described for the *in vitro* aggregation comparison experiment. Densitometric analysis of the stained FL αsyn protein band was conducted using the ImageJ program to quantify the percentage of FL αsyn insoluble protein for each sample at each time point.

EM analysis of C-truncated αsyn fibrils

αsyn fibrils prepared at 5 mg/ml underwent centrifugation at 100,000 × *g* for 30 min, and the fibril-containing pellet was suspended in microscopy grade water. Centrifugation was repeated twice to remove salts from the pellet, after which fibrils were adsorbed onto 300-mesh carbon-coated copper grids (Electron Microscopy Sciences, Hatfield, PA), negatively stained with 1% uranyl acetate, and visualized with a Hitachi 7600 transmission electron microscope. Fibril widths for at least 100 fibrils per truncation were measured by a blinded observer using Image Pro-Plus software (Media Cybernetics).

To investigate the possibility of mixed fibril formation between C-truncated and FL αsyn, fibrils were prepared at a total amount of 4 mg/ml but using 2 mg/ml human 21–140 αsyn and 2 mg/ml either the 1–115 or 1–129 human C-truncated forms of αsyn. A modified protocol for immunolabeling followed by EM was used (107). Fibrils were washed as described above and similarly adsorbed onto grids. The grids were blocked with 2% serum BSA in PBS for 10 min and sequentially incubated with primary antibodies diluted in 2% BSA/PBS; affinity-purified 4110 (20 μg/ml; residues 2–15 of αsyn) and 94-3A10 (20 μg/ml; residues 130–140) were used. Following washes with PBS, the grids were sequentially incubated with anti-mouse and anti-rabbit IgG secondary antibodies conjugated to 6 or 10 nm colloidal gold, respectively (Electron Microscopy Sciences, Hatfield, PA). Fibrils were negatively stained with 1% uranyl acetate and visualized with a Hitachi 7600 transmission electron microscope.

Proteolytic digestion of C-truncated αsyn fibrils

FL and C-truncated αsyn proteins were diluted to 5 mg/ml in sterile PBS (Invitrogen) and assembled into amyloid fibrils with continuous shaking at 1050 rpm and 37 °C for 5 days. For proteolytic digestion, 40 μg of each fibril was immediately diluted in sterile PBS to 1 mg/ml and incubated with either trypsin (Gibco) or proteinase K (Fisher) at two different concentrations for 30 min at 37 °C. Concentrations of proteases relative to the amount of fibrils were similar to previous studies (64, 65), with trypsin being used at 0.05 or 0.025 mg/ml and proteinase K being used at 0.005 or 0.0025 mg/ml. After 30 min, samples were placed on ice, and 1 mM phenylmethylsulfonyl fluoride was added to inhibit further digestion. SDS-sample buffer was added, and samples were heated to 100 °C for 10 min and resolved on SDS-PAGE. Gels were stained with Coomassie Blue R-250 to visualize digestion products.

Preparation of αsyn fibrils for seeding assays

For cell culture and animal experiments, FL or C-truncated αsyn proteins were diluted to 5 mg/ml in sterile PBS (Invitrogen) and assembled into amyloid fibrils with continuous shaking at 1050 rpm, 37 °C, for 5–7 days. Amyloid formation was confirmed by K114 and ThT fluorometry as described previously (60). Fibrils were diluted to 2 mg/ml and fragmented by gentle bath sonication for 60 min prior to seeding experiments. For mixed C-truncation/21–140 fibrils used in HEK293T seeding, the 21–140 protein and one each of the doubly N- and C-truncated proteins were fibrillized together in a 1:1 ratio and a total concentration of 5 mg/ml. For mixed C-truncation/FL fibrils in primary culture seeding, fibrils were produced similarly but using C-truncated and FL human fibrils without the 1–20 truncation.

Mammalian expression plasmids

The cDNA encoding FL human αsyn was previously cloned in the mammalian expression vector pcDNA3.1(+) (66). Plasmids encoding eight C-terminally truncated αsyn constructs were generated using the same mutagenic oligonucleotides as for the pRK172 plasmid to introduce premature stop codons to αsyn in the pcDNA3.1 plasmid. All mutations and the absence of errors throughout the entire length of the αsyn cDNA were confirmed by Sanger sequencing.

HEK293T cell culture and transfection

HEK293T cells were maintained in Dulbecco's modified Eagle's medium (Invitrogen) supplemented to contain 2 mM L-glutamine, 10% fetal bovine serum (FBS), 100 units/ml penicillin, and 100 μg/ml streptomycin, at 37 °C and 5% CO_2. Cells were plated into 4-cm^2 wells and allowed to reach 30–40% confluence, at which time cells were given fresh medium and transfected using a modified calcium phosphate protocol (66). For one well containing 1 ml of medium, 1.5 μg of pcDNA3.1 vector expressing either FL or C-truncated human αsyn was diluted in 18.75 μl of 0.25 M $CaCl_2$, after which the mixture was added stepwise into an equal volume of 2× BES buffer (50 mM *N*,*N*-bis(2-hydroxymethyl)-2-aminoethanesulfonic acid, 280 mM NaCl, 1.5 mM Na_2HPO_4, pH 6.96) to a final volume of 37.5 μl. The DNA-containing solution was incubated at room temperature for 15 min prior to adding it dropwise to the well. For co-transfection studies, pcDNA3.1 plasmids were diluted in 0.25 M $CaCl_2$ in a 1:1 ratio for a total of 1.5 μg of DNA/well. For seeding assays, preformed FL or C-truncated αsyn fibrils were added to 1 μM at 1 h after transfection, with the concentration being based on that of the monomeric subunits. At 16 h post-transfection, cells were washed with PBS, and medium was changed to Dulbecco's modified Eagle's medium culture medium containing 3% FBS. Cells were harvested for biochemical fractionation at a final time point of 64 h post-transfection. All sets of cell culture experiments for biochemical fractionation experiments were repeated at least one time.

HEK293T cell biochemical fractionation

HEK293T cells were washed once in PBS and subsequently lysed in 200 μl/well detergent extraction buffer (25 mM Tris-HCl, pH 7.5, 150 mM NaCl, 1 mM EDTA, 1% Triton X-100, 20 mM NaF) supplemented with protease inhibitors (1 mM phenylmethylsulfonyl fluoride and 1 mg/ml each of pepstatin, leupeptin, *N*-tosyl-L-phenylalanyl chloromethyl ketone, *N*-tosyl-lysine chloromethyl ketone, and soybean trypsin inhibitor). Detergent-insoluble material was sedimented at 100,000 × *g* for 30 min at 4 °C, and the supernatant was collected. To ensure complete removal of soluble material, centrifugation of the insoluble fraction was repeated before it was suspended in the same volume of detergent extraction buffer as the supernatant. Sample buffer was added to both fractions (10 mM Tris, pH 6.8, 1 mM EDTA, 40 mM DTT, 0.005% bromphenol blue, 0.0025% pyronin yellow, 1% SDS, 10% sucrose), and samples were boiled for 10 min. The insoluble fraction was additionally probe-sonicated for 1 min and boiled for an additional 10 min to ensure a homogenous solution prior to Western blot analysis.

Western blot analysis

Equal volumes of Triton-soluble and Triton-insoluble fractions were loaded onto 15% polyacrylamide gels and resolved by SDS-PAGE, followed by electrophoretic transfer onto 0.2-μm pore size nitrocellulose membranes (Bio-Rad) in carbonate transfer buffer (10 mM $NaHCO_3$, 3 mM Na_2CO_3, pH 9.9) (108). Membranes were blocked in 5% dry milk/Tris-buffered saline (TBS) and incubated overnight at 4 °C with primary antibody diluted in block solution. For experiments where C-truncated fibrils were added, the 94-3A10 antibody (residues 130–140) was utilized to avoid detection of exogenous fibrils. Similarly, the SNL-4 antibody (residues 2–12) was used when 21–140 fibrils or doubly N- and C-truncated fibrils were added, and mouse αsyn–specific antibodies D37A6 or 5G9 were used when human fibrils were added to neuronal-glial cultures expressing mouse αsyn. After washing in TBS, membranes were incubated in goat anti-rabbit or goat anti-mouse secondary antibodies conjugated to horseradish peroxidase (Jackson Immunoresearch Laboratories, Westgrove, PA) diluted in 5% dry milk/TBS for 1 h at room temperature; immunocomplexes were detected using Western Lightning-Plus ECL reagents (PerkinElmer Life Sciences) followed by chemiluminescence imaging (PXi, Syngene, Frederick, MD). Densitometry was performed using ImageJ software to quantify the ratio of detergent-insoluble to total αsyn. Quantified aggregation amounts used only experiments performed at the same time to reduce variability, although results were confirmed in additional replicate experiments.

Immunofluorescence of HEK293T cells

For immunofluorescence analysis, HEK293T cells were plated onto poly-D-lysine–coated glass coverslips. Transfection was performed with pcDNA3.1 vector expressing either FL or C-truncated human αsyn, and cells were subsequently treated with 1 μM 21–140 αsyn fibrils identically to biochemical fractionation experiments. 64 h after transfection, cells were rinsed with PBS and fixed with 4% paraformaldehyde for 10 min, followed by PBS washes. Cells were blocked with 5% FBS, PBS, 0.1% Triton X-100 for 30 min, followed by the application of primary antibodies Syn 506 and SNL4 diluted in block solution for 1 h at room temperature. Following PBS washes, fixed cells were then incubated with Alexa Fluor 488– and 594–conjugated secondary antibodies (Invitrogen) under the same conditions as for the primary antibody. Autofluorescence was quenched by application of 0.3% Sudan black for 10 min. Nuclei were counterstained with 4′,6-diamidino-2-phenylindole (DAPI; Invitrogen), and coverslips were mounted using Fluoromount-G (Southern Biotech, Birmingham, AL). Fluorescent images were captured using an Olympus BX51 fluorescence microscope mounted with a DP71 digital camera (Olympus, Center Valley, PA).

Mice

All animal experimental procedures were performed in adherence to University of Florida institutional animal care and use committee regulatory policies. Mice were housed under stable conditions with a 12-h light/dark cycle and access to food and water *ad libitum*. BALB/c mice were obtained from the Jackson Laboratory (Bar Harbor, MA), and C3HBL/6 mice were obtained from Charles River Laboratories (Wilmington, MA).

Production and validation of monoclonal antibodies selective for aggregated mouse αsyn

A peptide containing residues 117–129 of mouse αsyn along with an added N-terminal cysteine (CPVDPGSEAYEMPS) was synthesized by GenScript Inc. (Piscataway, NJ) and conjugated to mariculture keyhold limpet hemocyanin. Using this peptide, mice were immunized, followed by spleen harvest, hybridoma

fusion, and screening for reactivity to mouse but not human αsyn, as described previously (109). The positive clones were next screened by Western blotting of 200 ng of recombinant mouse and human αsyn or ~25 μg of cell culture lysate from HEK293T cells expressing mouse or human αsyn. Following validation of the antibodies for mouse αsyn specificity, immunohistochemistry was used to screen for antibodies that preferentially bound mouse αsyn in an aggregated state. Brains from C3HBL/6 mice known to contain pathologic inclusions after intrastriatal injection of mouse αsyn fibrils (81) were stained using hybridoma medium, as a number of these mice contain pathologic inclusions composed of mouse αsyn in the ipsilateral but not contralateral entorhinal cortex. Sections were observed for preferential staining of inclusions with low background staining of physiologic mouse αsyn. Tissue processing and sectioning as well as immunohistochemical antigen retrieval and staining were performed as described previously (110).

Primary neuronal-glial culture preparation

E16–18 C3HBL/6 mice were used to prepare primary mixed neuronal-glial cultures from cerebral cortices and maintained for 16 days total, as described previously (21). Cells were plated onto Nunc Lab-Tek II CC2 chamber slides (for immunofluorescence) or poly-D-lysine–coated 9-cm^2 wells (for biochemistry) at ~100,000–200,000 cells/cm^2. Cultures prepared using this method are usually 20% neuronal and 80% glial in composition (21). Cultures were maintained at 37 °C, 5% CO_2 in Neurobasal-A medium (Gibco) supplemented with 1% GlutaMax (Life Technologies), B-27, 100 units/ml penicillin, and 100 μg/ml streptomycin, with half the medium removed to fresh medium at day 2 and then every 4 days thereafter. Additionally, the initial plating medium contained 1% FBS.

Primary neuronal-glial culture seeding and aggregation assays

To study seeded aggregation in primary neuronal-glial cultures, preformed FL or C-truncated αsyn fibrils were used similarly to the HEK293T experiments. At culture day 6 following fresh medium change, recombinant αsyn fibrils were added to a final concentration of 1.5 μM, with the concentration being based on that of the monomeric subunits. Cells were then maintained for 10 more days and subsequently harvested for biochemical or immunofluorescence assays. Biochemical fractionation and Western blot analysis were performed as described for HEK293T cells. For double immunofluorescence analysis, cells were washed with PBS followed by fixation with 4% paraformaldehyde in PBS. Cells were subsequently blocked with 5% FBS, PBS, 0.1% Triton X-100 and then incubated for 1 h at room temperature with primary antibodies prepared in the block solution. Primary antibodies used for these experiments were the Tuj-1 or T2200 antibody for neuronal-specific βIII tubulin combined with either EP1536Y for $pSer^{129}$ or 5G9 against aggregated mouse αsyn. Following PBS washes, fixed cells were then incubated with Alexa Fluor 488– and 594–conjugated secondary antibodies (Invitrogen) under the same conditions as for the primary antibody. Nuclei were counterstained with DAPI (Invitrogen), and coverslips were mounted using Fluoromount-G (Southern Biotech). Fluorescent images were captured using an Olympus BX51 fluorescence microscope mounted with a DP71 digital camera (Olympus).

Quantitative analysis

Western blotting and SDS-PAGE data for aggregation comparison were quantified by ImageJ software (National Institutes of Health, Bethesda, MD). The insoluble αsyn fraction was reported as the ratio of the intensity of the αsyn band in the insoluble fraction divided by the summed intensities of αsyn in the soluble and insoluble fractions. Densitometric comparisons were performed in GraphPad Prism software using either one-way or two-way analysis of variance (ANOVA), with post hoc analysis using Dunnett's test to compare each truncation with the FL control.

For fluorometry data, spectroscopic readings for each replicate sample were blank-subtracted and averaged before using two-way ANOVA, with post hoc analysis using Dunnett's test to compare the normalized fluorescence of each truncation at each time point with the FL control.

Author contributions—Z. A. S. conducted experiments, analyzed the results, and contributed to the experimental designs and writing of the manuscript. N. V., K.-M. G., C. J. R., K. H. S., and J. C. conducted experiments. B. I. G. contributed to writing the manuscript and the experimental designs.

References

1. Spillantini, M. G., Crowther, R. A., Jakes, R., Hasegawa, M., and Goedert, M. (1998) α-Synuclein in filamentous inclusions of Lewy bodies from Parkinson's disease and dementia with Lewy bodies. *Proc. Natl. Acad. Sci. U.S.A.* **95,** 6469–6473
2. Uchihara, T., and Giasson, B. I. (2016) Propagation of α-synuclein pathology: hypotheses, discoveries, and yet unresolved questions from experimental and human brain studies. *Acta Neuropathol.* **131,** 49–73 CrossRef Medline
3. Lim, S., Chun, Y., Lee, J. S., and Lee, S.-J. (2016) Neuroinflammation in synucleinopathies. *Brain Pathol.* **26,** 404–409 CrossRef Medline
4. Goedert, M., Spillantini, M. G., Del Tredici, K., and Braak, H. (2013) 100 years of Lewy pathology. *Nat. Rev. Neurol.* **9,** 13–24 CrossRef Medline
5. Polymeropoulos, M. H., Lavedan, C., Leroy, E., Ide, S. E., Dehejia, A., Dutra, A., Pike, B., Root, H., Rubenstein, J., Boyer, R., Stenroos, E. S., Chandrasekharappa, S., Athanassiadou, A., Papapetropoulos, T., Johnson, W. G., *et al.* (1997) Mutation in the α-synuclein gene identified in families with Parkinson's disease. *Science* **276,** 2045–2047 CrossRef Medline
6. Deng, H., Wang, P., and Jankovic, J. (2018) The genetics of Parkinson disease. *Ageing Res. Rev.* **42,** 72–85 CrossRef Medline
7. Conway, K. A., Harper, J. D., and Lansbury, P. T. (1998) Accelerated *in vitro* fibril formation by a mutant α-synuclein linked to early-onset Parkinson disease. *Nat. Med.* **4,** 1318–1320 CrossRef Medline
8. Greenbaum, E. A., Graves, C. L., Mishizen-Eberz, A. J., Lupoli, M. A., Lynch, D. R., Englander, S. W., Axelsen, P. H., and Giasson, B. I. (2005) The E46K mutation in α-synuclein increases amyloid fibril formation. *J. Biol. Chem.* **280,** 7800–7807 CrossRef Medline
9. Khalaf, O., Fauvet, B., Oueslati, A., Dikiy, I., Mahul-Mellier, A.-L., Ruggeri, F. S., Mbefo, M. K., Vercruysse, F., Dietler, G., Lee, S.-J., Eliezer, D., and Lashuel, H. A. (2014) The H50Q mutation enhances α-synuclein aggregation, secretion, and toxicity. *J. Biol. Chem.* **289,** 21856–21876 CrossRef Medline
10. Giasson, B. I., Duda, J. E., Quinn, S. M., Zhang, B., Trojanowski, J. Q., and Lee, V. M.-Y. (2002) Neuronal α-synucleinopathy with severe movement

disorder in mice expressing A53T human α-synuclein. *Neuron* **34,** 521–533 CrossRef Medline

11. Emmer, K. L., Waxman, E. A., Covy, J. P., and Giasson, B. I. (2011) E46K human α-synuclein transgenic mice develop Lewy-like and tau pathology associated with age-dependent, detrimental motor impairment. *J. Biol. Chem.* **286,** 35104–35118 CrossRef Medline
12. Goedert, M., Masuda-Suzukake, M., and Falcon, B. (2017) Like prions: the propagation of aggregated tau and α-synuclein in neurodegeneration. *Brain* **140,** 266–278 CrossRef Medline
13. Kordower, J. H., Chu, Y., Hauser, R. A., Freeman, T. B., and Olanow, C. W. (2008) Lewy body-like pathology in long-term embryonic nigral transplants in Parkinson's disease. *Nat. Med.* **14,** 504–506 CrossRef Medline
14. Desplats, P., Lee, H.-J., Bae, E.-J., Patrick, C., Rockenstein, E., Crews, L., Spencer, B., Masliah, E., and Lee, S.-J. (2009) Inclusion formation and neuronal cell death through neuron-to-neuron transmission of α-synuclein. *Proc. Natl. Acad. Sci. U.S.A.* **106,** 13010–13015 CrossRef Medline
15. Valdinocci, D., Radford, R. A. W., Siow, S. M., Chung, R. S., and Pountney, D. L. (2017) Potential modes of intercellular α-synuclein transmission. *Int. J. Mol. Sci.* **18,** E469 Medline
16. Wong, Y. C., and Krainc, D. (2017) α-Synuclein toxicity in neurodegeneration: mechanism and therapeutic strategies. *Nat. Med.* **23,** 1–13 CrossRef Medline
17. Iljina, M., Garcia, G. A., Horrocks, M. H., Tosatto, L., Choi, M. L., Ganzinger, K. A., Abramov, A. Y., Gandhi, S., Wood, N. W., Cremades, N., Dobson, C. M., Knowles, T. P. J., and Klenerman, D. (2016) Kinetic model of the aggregation of α-synuclein provides insights into prion-like spreading. *Proc. Natl. Acad. Sci. U.S.A.* **113,** E1206–E1215 CrossRef Medline
18. Buell, A. K., Galvagnion, C., Gaspar, R., Sparr, E., Vendruscolo, M., Knowles, T. P. J., Linse, S., and Dobson, C. M. (2014) Solution conditions determine the relative importance of nucleation and growth processes in α-synuclein aggregation. *Proc. Natl. Acad. Sci. U.S.A.* **111,** 7671–7676 CrossRef Medline
19. Pinotsi, D., Buell, A. K., Galvagnion, C., Dobson, C. M., Kaminski Schierle, G. S., and Kaminski, C. F. (2014) Direct observation of heterogeneous amyloid fibril growth kinetics via two-color super-resolution microscopy. *Nano Lett.* **14,** 339–345 CrossRef Medline
20. Jang, A., Lee, H.-J., Suk, J.-E., Jung, J.-W., Kim, K.-P., and Lee, S.-J. (2010) Non-classical exocytosis of α-synuclein is sensitive to folding states and promoted under stress conditions. *J. Neurochem.* **113,** 1263–1274 Medline
21. Sacino, A. N., Brooks, M. M., Chakrabarty, P., Saha, K., Khoshbouei, H., Golde, T. E., and Giasson, B. I. (2017) Proteolysis of α-synuclein fibrils in the lysosomal pathway limits induction of inclusion pathology. *J. Neurochem.* **140,** 662–678 CrossRef Medline
22. McGlinchey, R. P., and Lee, J. C. (2015) Cysteine cathepsins are essential in lysosomal degradation of α-synuclein. *Proc. Natl. Acad. Sci. U.S.A.* **112,** 9322–9327 CrossRef Medline
23. Cuervo, A. M., Stefanis, L., Fredenburg, R., Lansbury, P. T., and Sulzer, D. (2004) Impaired degradation of mutant α-synuclein by chaperone-mediated autophagy. *Science* **305,** 1292–1295 CrossRef Medline
24. Fernandes, H. J. R., Hartfield, E. M., Christian, H. C., Emmanoulidou, E., Zheng, Y., Booth, H., Bogetofte, H., Lang, C., Ryan, B. J., Sardi, S. P., Badger, J., Vowles, J., Evetts, S., Tofaris, G. K., Vekrellis, K., *et al.* (2016) ER stress and autophagic perturbations lead to elevated extracellular α-synuclein in GBA-N370S Parkinson's iPSC-derived dopamine neurons. *Stem Cell Rep.* **6,** 342–356 CrossRef Medline
25. Wong, Y. C., and Krainc, D. (2016) Lysosomal trafficking defects link Parkinson's disease with Gaucher's disease. *Mov. Disord.* **31,** 1610–1618 CrossRef Medline
26. Bae, E.-J., Yang, N. Y., Lee, C., Kim, S., Lee, H.-J., and Lee, S.-J. (2015) Haploinsufficiency of cathepsin D leads to lysosomal dysfunction and promotes cell-to-cell transmission of α-synuclein aggregates. *Cell Death Dis.* **6,** e1901 CrossRef Medline
27. Robak, L. A., Jansen, I. E., van Rooij, J., Uitterlinden, A. G., Kraaij, R., Jankovic, J., International Parkinson's Disease Genomics Consortium (IPDGC), Heutink, P., Shulman, J. M., Nalls, M. A., Plagnol, V., Hernandez, D. G., Sharma, M., Sheerin, U.-M., Saad, M., *et al.* (2017) Excessive burden of lysosomal storage disorder gene variants in Parkinson's disease. *Brain* **140,** 3191–3203 CrossRef Medline
28. Kaushik, S., and Cuervo, A. M. (2018) The coming of age of chaperone-mediated autophagy. *Nat. Rev. Mol. Cell Biol.* **19,** 365–381 CrossRef Medline
29. Klein, A. D., and Mazzulli, J. R. (2018) Is Parkinson's disease a lysosomal disorder? *Brain* **141,** 2255–2262 CrossRef Medline
30. Sevlever, D., Jiang, P., and Yen, S.-H. C. (2008) Cathepsin D is the main lysosomal enzyme involved in the degradation of α-synuclein and generation of its carboxy-terminally truncated species. *Biochemistry* **47,** 9678–9687 CrossRef Medline
31. Tsujimura, A., Taguchi, K., Watanabe, Y., Tatebe, H., Tokuda, T., Mizuno, T., and Tanaka, M. (2015) Lysosomal enzyme cathepsin B enhances the aggregate forming activity of exogenous α-synuclein fibrils. *Neurobiol. Dis.* **73,** 244–253 CrossRef Medline
32. Pieri, L., Chafey, P., Le Gall, M., Clary, G., Melki, R., and Redeker, V. (2016) Cellular response of human neuroblastoma cells to α-synuclein fibrils, the main constituent of Lewy bodies. *Biochim. Biophys. Acta* **1860,** 8–19 CrossRef Medline
33. Hossain, S., Alim, A., Takeda, K., Kaji, H., Shinoda, T., and Uéda, K. (2001) Limited proteolysis of NACP/α-synuclein. *J. Alzheimers. Dis.* **3,** 577–584 CrossRef Medline
34. Zhang, Z., Kang, S. S., Liu, X., Ahn, E. H., Zhang, Z., He, L., Iuvone, P. M., Duong, D. M., Seyfried, N. T., Benskey, M. J., Manfredsson, F. P., Jin, L., Sun, Y. E., Wang, J.-Z., and Ye, K. (2017) Asparagine endopeptidase cleaves α-synuclein and mediates pathologic activities in Parkinson's disease. *Nat. Struct. Mol. Biol.* **24,** 632–642 CrossRef Medline
35. Murray, I. V. J., Giasson, B. I., Quinn, S. M., Koppaka, V., Axelsen, P. H., Ischiropoulos, H., Trojanowski, J. Q., and Lee, V. M.-Y. (2003) Role of α-synuclein carboxy-terminus on fibril formation *in vitro*. *Biochemistry* **42,** 8530–8540 CrossRef Medline
36. Crowther, R. A., Jakes, R., Spillantini, M. G., and Goedert, M. (1998) Synthetic filaments assembled from C-terminally truncated α-synuclein. *FEBS Lett.* **436,** 309–312 CrossRef Medline
37. Serpell, L. C., Berriman, J., Jakes, R., Goedert, M., and Crowther, R. A. (2000) Fiber diffraction of synthetic α-synuclein filaments shows amyloid-like cross-β conformation. *Proc. Natl. Acad. Sci. U.S.A.* **97,** 4897–4902 CrossRef Medline
38. Hoyer, W., Cherny, D., Subramaniam, V., and Jovin, T. M. (2004) Impact of the acidic C-terminal region comprising amino acids 109–140 on α-synuclein aggregation *in vitro*. *Biochemistry* **43,** 16233–16242 CrossRef Medline
39. Hoyer, W., Cherny, D., Subramaniam, V., and Jovin, T. M. (2004) Rapid self-assembly of α-synuclein observed by *in situ* atomic force microscopy. *J. Mol. Biol.* **340,** 127–139 CrossRef Medline
40. Mishizen-Eberz, A. J., Norris, E. H., Giasson, B. I., Hodara, R., Ischiropoulos, H., Lee, V. M.-Y., Trojanowski, J. Q., and Lynch, D. R. (2005) Cleavage of α-synuclein by calpain: potential role in degradation of fibrillized and nitrated species of α-synuclein. *Biochemistry* **44,** 7818–7829 CrossRef Medline
41. Iyer, A., Roeters, S. J., Kogan, V., Woutersen, S., Claessens, M. M. A. E., and Subramaniam, V. (2017) C-terminal truncated α-synuclein fibrils contain strongly twisted β-sheets. *J. Am. Chem. Soc.* **139,** 15392–15400 CrossRef Medline
42. Li, W., West, N., Colla, E., Pletnikova, O., Troncoso, J. C., Marsh, L., Dawson, T. M., Jäkälä, P., Hartmann, T., Price, D. L., and Lee, M. K. (2005) Aggregation promoting C-terminal truncation of α-synuclein is a normal cellular process and is enhanced by the familial Parkinson's disease-linked mutations. *Proc. Natl. Acad. Sci. U.S.A.* **102,** 2162–2167 CrossRef Medline
43. Liu, C.-W., Giasson, B. I., Lewis, K. A., Lee, V. M., Demartino, G. N., and Thomas, P. J. (2005) A precipitating role for truncated α-synuclein and the proteasome in α-synuclein aggregation: implications for pathogenesis of Parkinson disease. *J. Biol. Chem.* **280,** 22670–22678 CrossRef Medline
44. Baba, M., Nakajo, S., Tu, P. H., Tomita, T., Nakaya, K., Lee, V. M., Trojanowski, J. Q., and Iwatsubo, T. (1998) Aggregation of α-synuclein in

Lewy bodies of sporadic Parkinson's disease and dementia with Lewy bodies. *Am. J. Pathol.* **152,** 879–884 Medline

45. Anderson, J. P., Walker, D. E., Goldstein, J. M., de Laat, R., Banducci, K., Caccavello, R. J., Barbour, R., Huang, J., Kling, K., Lee, M., Diep, L., Keim, P. S., Shen, X., Chataway, T., Schlossmacher, M. G., *et al.* (2006) Phosphorylation of Ser-129 is the dominant pathological modification of α-synuclein in familial and sporadic Lewy body disease. *J. Biol. Chem.* **281,** 29739–29752 CrossRef Medline
46. Kellie, J. F., Higgs, R. E., Ryder, J. W., Major, A., Beach, T. G., Adler, C. H., Merchant, K., and Knierman, M. D. (2014) Quantitative measurement of intact α-synuclein proteoforms from post-mortem control and Parkinson's disease brain tissue by intact protein mass spectrometry. *Sci. Rep.* **4,** 5797 CrossRef Medline
47. Dufty, B. M., Warner, L. R., Hou, S. T., Jiang, S. X., Gomez-Isla, T., Leenhouts, K. M., Oxford, J. T., Feany, M. B., Masliah, E., and Rohn, T. T. (2007) Calpain-cleavage of α-synuclein: connecting proteolytic processing to disease-linked aggregation. *Am. J. Pathol.* **170,** 1725–1738 CrossRef Medline
48. Prasad, K., Beach, T. G., Hedreen, J., and Richfield, E. K. (2012) Critical role of truncated α-synuclein and aggregates in Parkinson's disease and incidental Lewy body disease. *Brain Pathol.* **22,** 811–825 CrossRef Medline
49. Hall, K., Yang, S., Sauchanka, O., Spillantini, M. G., and Anichtchik, O. (2015) Behavioural deficits in transgenic mice expressing human truncated (1–120 amino acid) α-synuclein. *Exp. Neurol.* **264,** 8–13 CrossRef Medline
50. Tofaris, G. K., Garcia Reitböck, P., Humby, T., Lambourne, S. L., O'Connell, M., Ghetti, B., Gossage, H., Emson, P. C., Wilkinson, L. S., Goedert, M., and Spillantini, M. G. (2006) Pathological changes in dopaminergic nerve cells of the substantia nigra and olfactory bulb in mice transgenic for truncated human α-synuclein(1–120): implications for Lewy body disorders. *J. Neurosci.* **26,** 3942–3950 CrossRef Medline
51. Michell, A. W., Tofaris, G. K., Gossage, H., Tyers, P., Spillantini, M. G., and Barker, R. A. (2007) The effect of truncated human α-synuclein (1–120) on dopaminergic cells in a transgenic mouse model of Parkinson's disease. *Cell Transplant.* **16,** 461–474 CrossRef Medline
52. Periquet, M., Fulga, T., Myllykangas, L., Schlossmacher, M. G., and Feany, M. B. (2007) Aggregated α-synuclein mediates dopaminergic neurotoxicity *in vivo*. *J. Neurosci.* **27,** 3338–3346 CrossRef Medline
53. Wakamatsu, M., Ishii, A., Iwata, S., Sakagami, J., Ukai, Y., Ono, M., Kanbe, D., Muramatsu, S., Kobayashi, K., Iwatsubo, T., and Yoshimoto, M. (2008) Selective loss of nigral dopamine neurons induced by overexpression of truncated human α-synuclein in mice. *Neurobiol. Aging* **29,** 574–585 CrossRef Medline
54. Daher, J. P. L., Ying, M., Banerjee, R., McDonald, R. S., Hahn, M. D., Yang, L., Flint Beal, M., Thomas, B., Dawson, V. L., Dawson, T. M., and Moore, D. J. (2009) Conditional transgenic mice expressing C-terminally truncated human α-synuclein (αSyn119) exhibit reduced striatal dopamine without loss of nigrostriatal pathway dopaminergic neurons. *Mol. Neurodegener.* **4,** 34 CrossRef Medline
55. Garcia-Reitböck, P., Anichtchik, O., Bellucci, A., Iovino, M., Ballini, C., Fineberg, E., Ghetti, B., Della Corte, L., Spano, P., Tofaris, G. K., Goedert, M., and Spillantini, M. G. (2010) SNARE protein redistribution and synaptic failure in a transgenic mouse model of Parkinson's disease. *Brain* **133,** 2032–2044 CrossRef Medline
56. Ulusoy, A., Febbraro, F., Jensen, P. H., Kirik, D., and Romero-Ramos, M. (2010) Co-expression of C-terminal truncated α-synuclein enhances full-length α-synuclein-induced pathology. *Eur. J. Neurosci.* **32,** 409–422 CrossRef Medline
57. Choi, D.-H., Kim, Y.-J., Kim, Y.-G., Joh, T. H., Beal, M. F., and Kim, Y.-S. (2011) Role of matrix metalloproteinase 3-mediated α-synuclein cleavage in dopaminergic cell death. *J. Biol. Chem.* **286,** 14168–14177 CrossRef Medline
58. Grassi, D., Howard, S., Zhou, M., Diaz-Perez, N., Urban, N. T., Guerrero-Given, D., Kamasawa, N., Volpicelli-Daley, L. A., LoGrasso, P., and Lasmézas, C. I. (2018) Identification of a highly neurotoxic α-synuclein species inducing mitochondrial damage and mitophagy in Parkinson's disease. *Proc. Natl. Acad. Sci. U.S.A.* **115,** E2634–E2643 CrossRef Medline
59. Conway, K. A., Harper, J. D., and Lansbury, P. T. (2000) Fibrils formed *in vitro* from α-synuclein and two mutant forms linked to Parkinson's disease are typical amyloid. *Biochemistry* **39,** 2552–2563 CrossRef Medline
60. Crystal, A. S., Giasson, B. I., Crowe, A., Kung, M.-P., Zhuang, Z.-P., Trojanowski, J. Q., and Lee, V. M.-Y. (2003) A comparison of amyloid fibrillogenesis using the novel fluorescent compound K114. *J. Neurochem.* **86,** 1359–1368 CrossRef Medline
61. Giasson, B. I., Murray, I. V. J., Trojanowski, J. Q., and Lee, V. M.-Y. (2001) A hydrophobic stretch of 12 amino acid residues in the middle of α-synuclein is essential for filament assembly. *J. Biol. Chem.* **276,** 2380–2386 CrossRef Medline
62. Vilar, M., Chou, H.-T., Lührs, T., Maji, S. K., Riek-Loher, D., Verel, R., Manning, G., Stahlberg, H., and Riek, R. (2008) The fold of α-synuclein fibrils. *Proc. Natl. Acad. Sci. U.S.A.* **105,** 8637–8642 CrossRef Medline
63. Tuttle, M. D., Comellas, G., Nieuwkoop, A. J., Covell, D. J., Berthold, D. A., Kloepper, K. D., Courtney, J. M., Kim, J. K., Barclay, A. M., Kendall, A., Wan, W., Stubbs, G., Schwieters, C. D., Lee, V. M. Y., George, J. M., and Rienstra, C. M. (2016) Solid-state NMR structure of a pathogenic fibril of full-length human α-synuclein. *Nat. Struct. Mol. Biol.* **23,** 409–415 CrossRef Medline
64. Guo, J. L., Covell, D. J., Daniels, J. P., Iba, M., Stieber, A., Zhang, B., Riddle, D. M., Kwong, L. K., Xu, Y., Trojanowski, J. Q., and Lee, V. M. Y. (2013) Distinct α-synuclein strains differentially promote tau inclusions in neurons. *Cell* **154,** 103–117 CrossRef Medline
65. Peng, C., Gathagan, R. J., Covell, D. J., Medellin, C., Stieber, A., Robinson, J. L., Zhang, B., Pitkin, R. M., Olufemi, M. F., Luk, K. C., Trojanowski, J. Q., and Lee, V. M.-Y. (2018) Cellular milieu imparts distinct pathological α-synuclein strains in α-synucleinopathies. *Nature* **557,** 558–563 CrossRef Medline
66. Waxman, E. A., and Giasson, B. I. (2010) A novel, high-efficiency cellular model of fibrillar α-synuclein inclusions and the examination of mutations that inhibit amyloid formation. *J. Neurochem.* **113,** 374–388 CrossRef Medline
67. Waxman, E. A., and Giasson, B. I. (2011) Induction of intracellular Tau aggregation is promoted by α-synuclein seeds and provides novel insights into the hyperphosphorylation of Tau. *J. Neurosci.* **31,** 7604–7618 CrossRef Medline
68. Strang, K. H., Croft, C. L., Sorrentino, Z. A., Chakrabarty, P., Golde, T. E., and Giasson, B. I. (2018) Distinct differences in prion-like seeding and aggregation between Tau protein variants provide mechanistic insights into tauopathies. *J. Biol. Chem.* **293,** 2408–2421 CrossRef Medline
69. Sacino, A. N., Brooks, M., McGarvey, N. H., McKinney, A. B., Thomas, M. A., Levites, Y., Ran, Y., Golde, T. E., and Giasson, B. I. (2013) Induction of CNS α-synuclein pathology by fibrillar and non-amyloidogenic recombinant α-synuclein. *Acta Neuropathol. Commun.* **1,** 38 CrossRef Medline
70. Sacino, A. N., Brooks, M., Thomas, M. A., McKinney, A. B., McGarvey, N. H., Rutherford, N. J., Ceballos-Diaz, C., Robertson, J., Golde, T. E., and Giasson, B. I. (2014) Amyloidogenic α-synuclein seeds do not invariably induce rapid, widespread pathology in mice. *Acta Neuropathol.* **127,** 645–665 CrossRef Medline
71. Sacino, A. N., Brooks, M., Thomas, M. A., McKinney, A. B., Lee, S., Regenhardt, R. W., McGarvey, N. H., Ayers, J. I., Notterpek, L., Borchelt, D. R., Golde, T. E., and Giasson, B. I. (2014) Intramuscular injection of α-synuclein induces CNS α-synuclein pathology and a rapid-onset motor phenotype in transgenic mice. *Proc. Natl. Acad. Sci. U.S.A.* **111,** 10732–10737 CrossRef Medline
72. Giasson, B. I., Jakes, R., Goedert, M., Duda, J. E., Leight, S., Trojanowski, J. Q., and Lee, V. M. Y. (2000) A panel of epitope-specific antibodies detects protein domains distributed throughout human α-synuclein in lewy bodies of Parkinson's disease. *J. Neurosci. Res.* **59,** 528–533 CrossRef Medline
73. Waxman, E. A., Duda, J. E., and Giasson, B. I. (2008) Characterization of antibodies that selectively detect α-synuclein in pathological inclusions. *Acta Neuropathol.* **116,** 37–46 CrossRef Medline
74. Rutherford, N. J., Dhillon, J. S., Riffe, C. J., Howard, J. K., Brooks, M., and Giasson, B. I. (2017) Comparison of the *in vivo* induction and transmis-

sion of α-synuclein pathology by mutant α-synuclein fibril seeds in transgenic mice. *Hum. Mol. Genet.* **26,** 4906–4915 CrossRef Medline
75. Bousset, L., Pieri, L., Ruiz-Arlandis, G., Gath, J., Jensen, P. H., Habenstein, B., Madiona, K., Olieric, V., Böckmann, A., Meier, B. H., and Melki, R. (2013) Structural and functional characterization of two α-synuclein strains. *Nat. Commun.* **4,** 2575 CrossRef Medline
76. Gath, J., Bousset, L., Habenstein, B., Melki, R., Böckmann, A., and Meier, B. H. (2014) Unlike twins: an NMR comparison of two α-synuclein polymorphs featuring different toxicity. *PLoS One* **9,** e90659 CrossRef Medline
77. Prusiner, S. B., Woerman, A. L., Mordes, D. A., Watts, J. C., Rampersaud, R., Berry, D. B., Patel, S., Oehler, A., Lowe, J. K., Kravitz, S. N., Geschwind, D. H., Glidden, D. V., Halliday, G. M., Middleton, L. T., Gentleman, S. M., *et al.* (2015) Evidence for α-synuclein prions causing multiple system atrophy in humans with parkinsonism. *Proc. Natl. Acad. Sci. U.S.A.* **112,** E5308–E5317 CrossRef Medline
78. Lemkau, L. R., Comellas, G., Lee, S. W., Rikardsen, L. K., Woods, W. S., George, J. M., and Rienstra, C. M. (2013) Site-specific perturbations of α-synuclein fibril structure by the Parkinson's disease associated mutations A53T and E46K. *PLoS One* **8,** e49750 CrossRef Medline
79. Ayers, J. I., Riffe, C. J., Sorrentino, Z. A., Diamond, J., Fagerli, E., Brooks, M., Galaleldeen, A., Hart, P. J., and Giasson, B. I. (2018) Localized induction of wild-type and mutant α-synuclein aggregation reveals propagation along neuroanatomical tracts. *J. Virol.* **92,** e00586-18 CrossRef Medline
80. Dhillon, J. S., Riffe, C., Moore, B. D., Ran, Y., Chakrabarty, P., Golde, T. E., and Giasson, B. I. (2017) A novel panel of α-synuclein antibodies reveal distinctive staining profiles in synucleinopathies. *PLoS One* **12,** e0184731 CrossRef Medline
81. Sorrentino, Z. A., Brooks, M. M. T., Hudson, V., 3rd, Rutherford, N. J., Golde, T. E., Giasson, B. I., and Chakrabarty, P. (2017) Intrastriatal injection of α-synuclein can lead to widespread synucleinopathy independent of neuroanatomic connectivity. *Mol. Neurodegener.* **12,** 40 CrossRef Medline
82. Muntané, G., Ferrer, I., and Martinez-Vicente, M. (2012) α-Synuclein phosphorylation and truncation are normal events in the adult human brain. *Neuroscience* **200,** 106–119 CrossRef Medline
83. Izawa, Y., Tateno, H., Kameda, H., Hirakawa, K., Hato, K., Yagi, H., Hongo, K., Mizobata, T., and Kawata, Y. (2012) Role of C-terminal negative charges and tyrosine residues in fibril formation of α-synuclein. *Brain Behav.* **2,** 595–605 CrossRef Medline
84. Afitska, K., Fucikova, A., Shvadchak, V. V., and Yushchenko, D. A. (2017) Modification of C terminus provides new insights into the mechanism of α-synuclein aggregation. *Biophys. J.* **113,** 2182–2191 CrossRef Medline
85. Park, S. M., Jung, H. Y., Chung, K. C., Rhim, H., Park, J. H., and Kim, J. (2002) Stress-induced aggregation profiles of GST-α-synuclein fusion proteins: role of the C-terminal acidic tail of α-synuclein in protein thermosolubility and stability. *Biochemistry* **41,** 4137–4146 CrossRef Medline
86. Park, S. M., Jung, H. Y., Kim, T. D., Park, J. H., Yang, C.-H., and Kim, J. (2002) Distinct roles of the N-terminal-binding domain and the C-terminal-solubilizing domain of α-synuclein, a molecular chaperone. *J. Biol. Chem.* **277,** 28512–28520 CrossRef Medline
87. McLean, P. J., and Hyman, B. T. (2002) An alternatively spliced form of rodent α-synuclein forms intracellular inclusions *in vitro*: role of the carboxy-terminus in α-synuclein aggregation. *Neurosci. Lett.* **323,** 219–223 CrossRef Medline
88. Bertoncini, C. W., Jung, Y.-S., Fernandez, C. O., Hoyer, W., Griesinger, C., Jovin, T. M., and Zweckstetter, M. (2005) Release of long-range tertiary interactions potentiates aggregation of natively unstructured α-synuclein. *Proc. Natl. Acad. Sci. U.S.A.* **102,** 1430–1435 CrossRef Medline
89. Yap, T. L., Pfefferkorn, C. M., and Lee, J. C. (2011) Residue-specific fluorescent probes of α-synuclein: detection of early events at the N- and C-termini during fibril assembly. *Biochemistry* **50,** 1963–1965 CrossRef Medline
90. Park, S., Yoon, J., Jang, S., Lee, K., and Shin, S. (2016) The role of the acidic domain of α-synuclein in amyloid fibril formation: a molecular dynamics study. *J. Biomol. Struct. Dyn.* **34,** 376–383 CrossRef Medline
91. El-Turk, F., Newby, F. N., De Genst, E., Guilliams, T., Sprules, T., Mittermaier, A., Dobson, C. M., and Vendruscolo, M. (2016) Structural effects of two camelid nanobodies directed to distinct C-terminal epitopes on α-synuclein. *Biochemistry* **55,** 3116–3122 CrossRef Medline
92. Meuvis, J., Gerard, M., Desender, L., Baekelandt, V., and Engelborghs, Y. (2010) The conformation and the aggregation kinetics of α-synuclein depend on the proline residues in its C-terminal region. *Biochemistry* **49,** 9345–9352 CrossRef Medline
93. Sugeno, N., Hasegawa, T., Tanaka, N., Fukuda, M., Wakabayashi, K., Oshima, R., Konno, M., Miura, E., Kikuchi, A., Baba, T., Anan, T., Nakao, M., Geisler, S., Aoki, M., and Takeda, A. (2014) Lys-63-linked ubiquitination by E3 ubiquitin ligase Nedd4-1 facilitates endosomal sequestration of internalized α-synuclein. *J. Biol. Chem.* **289,** 18137–18151 CrossRef Medline
94. Levitan, K., Chereau, D., Cohen, S. I. A., Knowles, T. P. J., Dobson, C. M., Fink, A. L., Anderson, J. P., Goldstein, J. M., and Millhauser, G. L. (2011) Conserved C-terminal charge exerts a profound influence on the aggregation rate of α-synuclein. *J. Mol. Biol.* **411,** 329–333 CrossRef Medline
95. Zibaee, S., Jakes, R., Fraser, G., Serpell, L. C., Crowther, R. A., and Goedert, M. (2007) Sequence determinants for amyloid fibrillogenesis of human α-synuclein. *J. Mol. Biol.* **374,** 454–464 CrossRef Medline
96. Vamvaca, K., Lansbury, P. T., Jr, and Stefanis, L. (2011) N-terminal deletion does not affect α-synuclein membrane binding, self-association and toxicity in human neuroblastoma cells, unlike yeast. *J. Neurochem.* **119,** 389–397 CrossRef Medline
97. Qin, Z., Hu, D., Han, S., Hong, D.-P., and Fink, A. L. (2007) Role of different regions of α-synuclein in the assembly of fibrils. *Biochemistry* **46,** 13322–13330 CrossRef Medline
98. Masaracchia, C., Hnida, M., Gerhardt, E., Lopes da Fonseca, T., Villar-Pique, A., Branco, T., Stahlberg, M. A., Dean, C., Fernández, C. O., Milosevic, I., and Outeiro, T. F. (2018) Membrane binding, internalization, and sorting of α-synuclein in the cell. *Acta Neuropathol. Commun.* **6,** 79 CrossRef Medline
99. Cremades, N., Cohen, S. I. A., Deas, E., Abramov, A. Y., Chen, A. Y., Orte, A., Sandal, M., Clarke, R. W., Dunne, P., Aprile, F. A., Bertoncini, C. W., Wood, N. W., Knowles, T. P. J., Dobson, C. M., and Klenerman, D. (2012) Direct observation of the interconversion of normal and toxic forms of α-synuclein. *Cell* **149,** 1048–1059 CrossRef Medline
100. Abdelmotilib, H., Maltbie, T., Delic, V., Liu, Z., Hu, X., Fraser, K. B., Moehle, M. S., Stoyka, L., Anabtawi, N., Krendelchtchikova, V., Volpicelli-Daley, L. A., and West, A. (2017) α-Synuclein fibril-induced inclusion spread in rats and mice correlates with dopaminergic neurodegeneration. *Neurobiol. Dis.* **105,** 84–98 CrossRef Medline
101. Luk, K. C., Covell, D. J., Kehm, V. M., Zhang, B., Song, I. Y., Byrne, M. D., Pitkin, R. M., Decker, S. C., Trojanowski, J. Q., and Lee, V. M.-Y. (2016) Molecular and biological compatibility with host α-synuclein influences fibril pathogenicity. *Cell Rep.* **16,** 3373–3387 CrossRef Medline
102. Terada, M., Suzuki, G., Nonaka, T., Kametani, F., Tamaoka, A., and Hasegawa, M. (2018) The effect of truncation on prion-like properties of α-synuclein. *J. Biol. Chem.* **293,** 13910–13920 CrossRef Medline
103. Chen, M., Margittai, M., Chen, J., and Langen, R. (2007) Investigation of α-synuclein fibril structure by site-directed spin labeling. *J. Biol. Chem.* **282,** 24970–24979 CrossRef Medline
104. Li, Y., Zhao, C., Luo, F., Liu, Z., Gui, X., Luo, Z., Zhang, X., Li, D., Liu, C., and Li, X. (2018) Amyloid fibril structure of α-synuclein determined by cryo-electron microscopy. *Cell Res.* **28,** 897–903 CrossRef Medline
105. Guerrero-Ferreira, R., Taylor, N. M., Mona, D., Ringler, P., Lauer, M. E., Riek, R., Britschgi, M., and Stahlberg, H. (2018) Cryo-EM structure of α-synuclein fibrils. *Elife* **7,** e36402 CrossRef Medline
106. Duda, J. E., Giasson, B. I., Mabon, M. E., Lee, V. M.-Y., and Trojanowski, J. Q. (2002) Novel antibodies to synuclein show abundant striatal pathology in Lewy body diseases. *Ann. Neurol.* **52,** 205–210 CrossRef Medline
107. Giasson, B. I., Forman, M. S., Higuchi, M., Golbe, L. I., Graves, C. L., Kotzbauer, P. T., Trojanowski, J. Q., and Lee, V. M.-Y. (2003) Initiation and synergistic fibrillization of tau and α-synuclein. *Science* **300,** 636–640 CrossRef Medline
108. Dunn, S. D. (1986) Effects of the modification of transfer buffer composition and the renaturation of proteins in gels on the recognition of pro-

teins on Western blots by monoclonal antibodies. *Anal. Biochem.* **157,** 144–153 CrossRef Medline

109. Strang, K. H., Goodwin, M. S., Riffe, C., Moore, B. D., Chakrabarty, P., Levites, Y., Golde, T. E., and Giasson, B. I. (2017) Generation and characterization of new monoclonal antibodies targeting the PHF1 and AT8 epitopes on human tau. *Acta Neuropathol. Commun.* **5,** 58 CrossRef Medline

110. Duda, J. E., Giasson, B. I., Gur, T. L., Montine, T. J., Robertson, D., Biaggioni, I., Hurtig, H. I., Stern, M. B., Gollomp, S. M., Grossman, M., Lee, V. M., and Trojanowski, J. Q. (2000) Immunohistochemical and biochemical studies demonstrate a distinct profile of α-synuclein permutations in multiple system atrophy. *J. Neuropathol. Exp. Neurol.* **59,** 830–841 CrossRef Medline